Nucleon-nucleon bremsstrahlung: Anomalous magnetic moment effects

R. G. E. Timmermans and T. D. Penninga
Theory Group, Kernfysisch Versneller Instituut, University of Groningen, Zernikelaan 25, NL-9747 AA Groningen, The Netherlands

B. F. Gibson
Theoretical Division, Los Alamos National Laboratory, Los Alamos, New Mexico 87545, USA

M. K. Liou
Department of Physics and Institute for Nuclear Theory, Brooklyn College of the City University of New York, Brooklyn, New York 11210, USA
(Received 29 September 2005; published 28 March 2006)

Background: Two soft-photon amplitudes, the two-u-two-t special (TuTts) amplitude and the Low amplitude, are known to produce quantitatively similar $np\gamma$ cross sections, but they predict quite different $pp\gamma$ cross sections for those kinematic conditions in which the nucleon scattering angles are small (less than 25°). ***Purpose:*** These two amplitudes have been applied to systematically investigate three different nucleon-nucleon bremsstrahlung ($NN\gamma$) processes: $pp\gamma$, $np\gamma$, and $nn\gamma$. The $nn\gamma$ process is explored for the first time. The primary focus of this work is to investigate the contribution of the proton and the neutron anomalous magnetic moments to all three $NN\gamma$ processes for projectile energies above 150 MeV and for laboratory scattering angles (θ_1 and θ_2) lying between 8° and 40°. ***Method***: A special soft-photon expansion in which the TuTts amplitude is expanded in terms of the Low amplitude plus additional amplitudes is utilized to explore the relationship between the TuTts and Low amplitudes and the reasons why they agree and disagree. We also used the TuTts amplitude to calculate the $NN\gamma$ cross section with and without the anomalous magnetic moment contributions to explore the importance of that element of the electromagnetic current. ***Results:*** The TuTts amplitude describes well the available $pp\gamma$ cross-section data. The anomalous magnetic moment contribution is (i) significant in the $pp\gamma$ process when each scattering angle is less than 25° but insignificant when each scattering angle is 40° or greater and (ii) insignificant in the $np\gamma$ process for all scattering angles. The $nn\gamma$ cross sections for the TuTts and Low amplitudes differ substantially for the kinematics investigated. ***Conclusions:*** In general, the Low amplitude agrees well with the TuTts amplitude when anomalous magnetic moment effects are not significant, but the two amplitudes can yield quite different predictions when such effects are significant. These findings have enhanced our understanding of the fundamental emission mechanism governing $NN\gamma$ processes, and they explain why the TuTts amplitude should be used to describe all three $NN\gamma$ processes.

DOI: 10.1103/PhysRevC.73.034006 PACS number(s): 21.30.Cb, 25.20.−x

I. INTRODUCTION

The effect of the nucleon anomalous magnetic moments in nucleon-nucleon bremsstrahlung ($NN\gamma$, including $pp\gamma$, $np\gamma$, and $nn\gamma$) has received renewed attention because it has been found to play an important role in our understanding of the fundamental photon emission mechanism governing bremsstrahlung in the two-nucleon scattering process. The anomalous magnetic moment effect in $pp\gamma$ has been studied using the nonrelativistic potential model approach [1]. Most recently, utilizing two different relativistic soft-photon amplitudes (the two-u-two-t special amplitude M_μ^{TuTts} and the Low [2] amplitude M_μ^{Low}), the effect was investigated in both $pp\gamma$ and $np\gamma$ processes [3]. The most interesting results can be summarized as follows: (i) The anomalous magnetic moment contribution to the $pp\gamma$ cross section was found to be significant while that to the $np\gamma$ cross section was found to be insignificant. (ii) The amplitude M_μ^{TuTts} retains most of the essential contribution from the terms in the soft-photon expansion which depend upon the anomalous magnetic moments. The primary difference between M_μ^{TuTts} and M_μ^{Low} is that the former includes an additional term $M_\mu^{(3)}(K^1;\kappa)$, which is of order K in the photon energy and is a function of the anomalous magnetic moments. (iii) For the $pp\gamma$ process, the M_μ^{TuTts} amplitude provides a better soft-photon approximation than does the M_μ^{Low} amplitude, because the contribution coming from $M_\mu^{(3)}(K^1;\kappa)$ can be important in the calculation of the $pp\gamma$ cross sections. In fact, the success of the M_μ^{TuTts} approximation in describing the available $pp\gamma$ data has been well established; for that reason, M_μ^{TuTts} is the preferred soft-photon amplitude for investigating the role of the proton anomalous magnetic moment in that process. (iv) For the $np\gamma$ process, M_μ^{TuTts} and M_μ^{Low} provide approximately equivalent results, because the contribution from both $M_\mu^{(3)}(K^1;\kappa)$ and the other magnetic-moment-dependent amplitude $M_\mu^{\mathrm{mag}}(K^0;\kappa)$ are essentially negligible, so that the two soft-photon amplitudes predict quantitatively similar $np\gamma$ cross sections. (v) In addition to showing interesting results for $pp\gamma$ and $np\gamma$, Ref. [3]

has introduced a new soft-photon expansion in which the amplitude M_μ^{TuTts} is expanded in terms of several special amplitudes [M_μ^{Low}, $M_\mu^{(1)}(K^{-1};e)$, $M_\mu^{\mathrm{mag}}(K^0;\kappa)$, $M_\mu^{\mathrm{ex}}(K^0)$, and $M_\mu^{(3)}(K^1;\kappa)$; see Eq. (1) of Ref. [3]]. This expansion provides a useful method which can be utilized to analyze experimental data and to investigate the contributions of those special amplitudes to $NN\gamma$. This method has been employed in our investigation reported here.

In order to explore completely the effect of anomalous magnetic moments in the $NN\gamma$ process, we must include $nn\gamma$ in our investigations. Therefore, we have systematically investigated these effects in $pp\gamma$, $np\gamma$, and $nn\gamma$. We have used the amplitudes M_μ^{TuTts} and M_μ^{Low}, as defined in Sec. II, to calculate coplanar $NN\gamma$ cross sections $d^3\sigma/d\Omega_1 d\Omega_2 d\psi_\gamma$ as functions of the photon angle ψ_γ for several laboratory nucleon projectile energies above 150 MeV and for laboratory scattering angles between 8° and 40°. For the $pp\gamma$ case, we present calculations to support our previous finding that the contribution from the proton anomalous magnetic moment dominates the cross section. Moreover, to clearly demonstrate that the contribution from $M_\mu^{(3)}(K^1;\kappa)$ is important in the $pp\gamma$ process, we compare results for three new amplitudes [$M_{(1)\mu}^{\mathrm{TuTts}}$, $M_{(2)\mu}^{\mathrm{TuTts}}$, and $M_{(3)\mu}^{\mathrm{TuTts}}$] defined in Sec. II to calculate $pp\gamma$ cross sections. These results not only explain why the M_μ^{TuTts} calculation agrees well with the available $pp\gamma$ cross-section data but also provide an explanation for discrepancies between the data and calculations using the M_μ^{Low} amplitude. In contrast, our investigation shows for the $np\gamma$ case that the overall contribution from the anomalous magnetic moments [including $M_\mu^{(3)}(K^1;\kappa)$] is consistently small for the kinematics investigated. Our numerical results suggest that the insignificant anomalous magnetic moment effect in the $np\gamma$ process may arise from a cancellation between the contribution from the anomalous magnetic moment of the proton and that of the neutron. Because the anomalous magnetic moment effect is small, contributions from meson-exchange current effects play a much larger role in $np\gamma$ cross-section calculations.

The $nn\gamma$ process has not been previously investigated systematically. Although free-space nn scattering is not directly observable in the laboratory, the $nn\gamma$ process does contribute to nucleus-nucleus bremsstrahlung (even though the most important contribution comes from the $E1$-dominated $np\gamma$ process). Because the neutron has zero charge, the two soft-photon amplitudes M_μ^{TuTts} and M_μ^{Low} (and the resulting $nn\gamma$ cross sections) can only depend upon the anomalous magnetic moment of the neutron. This is an ideal situation in which to investigate without ambiguity the anomalous magnetic moment effect and the contribution of $M_\mu^{(3)}(K^1)$. It is understood that if the contribution of $M_\mu^{(3)}(K^1)$ is significant, then M_μ^{TuTts} and M_μ^{Low} will yield very different $nn\gamma$ cross-section predictions. In that case, M_μ^{TuTts} should be used to describe the $nn\gamma$ process. We also compare calculated $pp\gamma$ and $nn\gamma$ cross sections, in order to investigate similarities and differences in the two processes.

Our presentation is organized as follows: In Sec. II, we define the amplitude M_μ^{TuTts} for $pp\gamma$, $np\gamma$, and $nn\gamma$ processes. We derive an explicit relationship between M_μ^{TuTts} and M_μ^{Low}. We also define three additional amplitudes [$M_{(1)\mu}^{\mathrm{TuTts}}$, $M_{(2)\mu}^{\mathrm{TuTts}}$, and $M_{(3)\mu}^{\mathrm{TuTts}}$] to be used in the investigation of the $M_\mu^{(3)}(K^1)$ contribution. In Sec. III, we present our numerical results. We also discuss their implications. Our conclusions are summarized in Sec. IV. In the Appendix, we outline how the M_μ^{TuTts} amplitude for $np\gamma$ and $nn\gamma$ processes is derived.

II. THE NUCLEON-NUCLEON BREMSSTRAHLUNG AMPLITUDE

Consider photon emission accompanying the scattering of two nucleons N_1 and N_2,

$$N_1\left(P_1^\mu\right) + N_2\left(P_2^\mu\right) \to N_1\left(P_1'^\mu\right) + N_2\left(P_2'^\mu\right) + \gamma(K^\mu), \tag{1}$$

where N_i ($i = 1, 2$) can be either a proton p or a neutron n, P_1^μ (P_2^μ) is the four-momentum of the incident (target) nucleon, $P_1'^\mu$ ($P_2'^\mu$) is the four-momentum of the scattered (recoil) nucleon, and K^μ is the four-momentum of the emitted photon with polarization ϵ^μ. Equation (1) describes three distinct NN bremsstrahlung processes: $pp\gamma$, $np\gamma$, and $nn\gamma$. Each nucleon N_i ($i = 1, 2$) has mass m, charge e_i, and anomalous magnetic moment κ_i. Here, $e_i = e$ for a proton and 0 (zero) for a neutron, while $\kappa_i = \kappa_p = +1.793$ for a proton and $\kappa_i = \kappa_n = -1.913$ for a neutron. The five four-momenta comprising Eq. (1), which satisfy the energy-momentum conservation defined by

$$P_1^\mu + P_2^\mu = P_1'^\mu + P_2'^\mu + K^\mu, \tag{2}$$

can be used to define six Mandelstam variables for NN bremsstrahlung processes:

$$\begin{aligned} s_i &= (P_1 + P_2)^2, \quad & s_f &= (P_1' + P_2')^2, \\ t_1 &= (P_1' - P_1)^2, \quad & t_2 &= (P_2' - P_2)^2, \\ u_1 &= (P_2' - P_1)^2, \quad & u_2 &= (P_1' - P_2)^2. \end{aligned} \tag{3}$$

A. The NN elastic scattering amplitudes

When the photon momentum K approaches zero, the three NN bremsstrahlung processes depicted in Eq. (1) reduce to the corresponding NN elastic scattering processes,

$$N_1\left(P_1^\mu\right) + N_2\left(P_2^\mu\right) \to N_1\left(\bar{P}_1'^\mu\right) + N_2\left(\bar{P}_2'^\mu\right), \tag{4}$$

where

$$\bar{P}_1'^\mu = \lim_{K\to 0} P_1'^\mu, \quad \bar{P}_2'^\mu = \lim_{K\to 0} P_2'^\mu, \tag{5}$$

and the six Mandelstam variables defined by Eq. (3) reduce to three variables s, t, and u:

$$\begin{aligned} s &= s_i = \lim_{K\to 0} s_f, \\ t &= \lim_{K\to 0} t_1 = \lim_{K\to 0} t_2, \\ u &= \lim_{K\to 0} u_1 = \lim_{K\to 0} u_2. \end{aligned} \tag{6}$$

The fact that these three variables satisfy the on-shell condition,

$$s + t + u = 4m^2, \tag{7}$$

implies that only two are independent. We employ a covariant *NN* elastic scattering amplitude obtained by Goldberger, Grisaru, MacDowell, and Wong (GGMW) [4] as the input for our bremsstrahlung calculations. The GGMW amplitude has the form [5]

$$F = \sum_{\alpha=1}^{5} F_\alpha[G_\alpha + (-1)^\alpha \widetilde{G}_\alpha], \tag{8}$$

where

$$\begin{aligned} G_\alpha &= \bar{u}(\bar{P}_1')\lambda_\alpha u(P_1)\bar{u}(\bar{P}_2')\lambda^\alpha u(P_2),\\ \widetilde{G}_\alpha &= \bar{u}(\bar{P}_2')\lambda_\alpha u(P_1)\bar{u}(\bar{P}_1')\lambda^\alpha u(P_2), \end{aligned} \tag{9}$$

and the tensors λ_α and λ^α are defined by

$$\begin{aligned} (\lambda_1, \lambda_2, \lambda_3, \lambda_4, \lambda_5) &= \left(1, \frac{\sigma_{\mu\nu}}{\sqrt{2}}, i\gamma_5\gamma_\mu, \gamma_\mu, \gamma_5\right),\\ (\lambda^1, \lambda^2, \lambda^3, \lambda^4, \lambda^5) &= \left(1, \frac{\sigma^{\mu\nu}}{\sqrt{2}}, i\gamma_5\gamma^\mu, \gamma^\mu, \gamma_5\right). \end{aligned} \tag{10}$$

In Eq. (8), F_α ($\alpha = 1, 2, 3, 4, 5$) are invariant functions of two independent variables chosen from *s, t,* and *u*. Because the GGMW amplitude will be used to construct the two-*u*-two-*t* special (TuTts) amplitude for the *NN* bremsstrahlung process, we choose *u* and *t* to be the two independent variables, and we write $F_\alpha = F_\alpha(u, t)$. Furthermore, for states belonging to the isotopic triplet (*pp* and *nn*), we impose the condition

$$F_\alpha(u, t) = (-1)^{\alpha+1} F_\alpha(t, u), \tag{11}$$

so that the amplitude F, as given by Eq. (8), will obey the Pauli principle [5]. [The condition for the isotopic singlet state is $F_\alpha(u, t) = (-1)^\alpha F_\alpha(t, u)$.]

If we apply the Fierz transformation, $\widetilde{G}_\alpha$ ($\alpha = 1, 2, 3, 4, 5$) can be expressed in terms of G_α, and the amplitude F can be written as

$$F = \sum_{\alpha=1}^{5} F^e_\alpha(u, t) G_\alpha, \tag{12}$$

where the invariant functions $F^e_\alpha(u, t)$ are defined in terms of invariant functions $F_\alpha(u, t)$. [See Eq. (48) of Ref. [5].]

B. The two-*u*-two-*t* special amplitude

The *NN* elastic scattering amplitude F given by Eq. (12) has been used to construct the TuTts amplitudes for *NN* bremsstrahlung processes. They are given by the following expressions:

$$\begin{aligned} M^{\rm TuTts}_\mu = \sum_{\alpha=1}^{5} \big[&\bar{u}(P_1')X_{\mu\alpha}u(P_1)\bar{u}(P_2')\lambda^\alpha u(P_2)\\ &+ \bar{u}(P_1')\lambda^\alpha u(P_1)\bar{u}(P_2')Y_{\mu_\alpha} u(P_2)\big], \end{aligned} \tag{13}$$

where

$$\begin{aligned} X_{\mu\alpha} &= F^e_\alpha(u_1, t_2)\left[\frac{e_1 P'_{1\mu} + R^{P_1'}_{1\mu}}{P_1' \cdot K} - V_{x\mu}\right]\lambda_\alpha\\ &\quad - F^e_\alpha(u_2, t_2)\lambda_\alpha\left[\frac{e_1 P_{1\mu} + R^{P_1}_{1\mu}}{P_1 \cdot K} - V_{x\mu}\right],\\ Y_{\mu\alpha} &= F^e_\alpha(u_2, t_1)\left[\frac{e_2 P'_{2\mu} + R^{P_2'}_{2\mu}}{P_2' \cdot K} - V_{y\mu}\right]\lambda_\alpha\\ &\quad - F^e_\alpha(u_1, t_1)\lambda_\alpha\left[\frac{e_2 P_{2\mu} + R^{P_2}_{2\mu}}{P_2 \cdot K} - V_{y\mu}\right], \end{aligned} \tag{14}$$

in terms of

$$\begin{aligned} R^{P_1'}_{1\mu} &= \frac{e_1}{4}[\gamma_\mu, \not{K}] + \frac{\kappa_1}{8m}\{[\gamma_\mu, \not{K}], \not{P}_1'\},\\ R^{P_1}_{1\mu} &= R^{P_1'}_{1\mu}(P_1' \to P_1),\\ R^{P_2'}_{2\mu} &= \frac{e_2}{4}[\gamma_\mu, \not{K}] + \frac{\kappa_2}{8m}\{[\gamma_\mu, \not{K}], \not{P}_2'\},\\ R^{P_2}_{2\mu} &= R^{P_2'}_{2\mu}(P_2' \to P_2), \end{aligned}$$

and we have used $[A, B] \equiv AB - BA$ and $\{A, B\} \equiv AB + BA$. The $V_{x\mu}$ and $V_{y\mu}$ can be either V_μ or V'_μ, where

$$\begin{aligned} V_\mu &= e\left[\frac{(P_2 - P_2')_\mu}{(2P_2 - P_2') \cdot K} + \frac{(P_1 - P_2')_\mu}{2(P_1 - P_2') \cdot K}\right],\\ V'_\mu &= e\left[\frac{(P_2 - P_2')_\mu}{2(P_2 - P_2') \cdot K} - \frac{(P_1 - P_2')_\mu}{2(P_1 - P_2') \cdot K}\right]. \end{aligned} \tag{15}$$

More precisely, Eq. (13) represents three different amplitudes:

(i) For the $pp\gamma$ process, $e_1 = e_2 = e, \kappa_1 = \kappa_2 = \kappa_p$, and $V_{x\mu} = V_{y\mu} = V_\mu$.
(ii) For the $np\gamma$ process, $e_1 = 0, e_2 = e, \kappa_1 = \kappa_n, \kappa_2 = \kappa_p$, $V_{x\mu} = V'_\mu$, and $V_{y\mu} = V_\mu$.
(iii) For the $nn\gamma$ process, $e_1 = e_2 = 0, \kappa_1 = \kappa_2 = \kappa_n$, and $V_{x,\mu} = V_{y\mu} = 0$.

It is easily shown that $M^{\rm TuTts}_\mu$ satisfies the gauge invariant condition, $K^\mu M^{\rm TuTts}_\mu = 0$.

The amplitude $M^{\rm TuTts}_\mu$ given by Eq. (13) for the $pp\gamma$ process is identical to the amplitude $M^{\rm TuTts}_{1\mu}$ given in Eq. (49) of Ref. [5]. As discussed in Appendix A, we have followed the method used in Ref. [5] to derive the amplitude $M^{\rm TuTts}_\mu$ for both $np\gamma$ and $nn\gamma$ processes. Because the neutron has no charge and the external amplitude for the $nn\gamma$ process is already gauge invariant, the amplitude $M^{\rm TuTts}_\mu$ involves no additional gauge term.

Equation (13) plus the first two equations in Eq. (14) show that $M^{\rm TuTts}_\mu$ depends on the invariant functions F^e_α evaluated at four on-shell points (u_i, t_j) for $i, j = 1, 2$. To help one understand how and why (u_i, t_j) have been chosen as the on-shell points for the amplitude $M^{\rm TuTts}_\mu$, we should first point out that there are several options for choosing the on-shell conditions. There are four different external photon emission processes, because a photon can be emitted from any one of the four nucleon legs in a given *NN* bremsstrahlung process.

The external amplitude is, therefore, a sum of four different half-off-shell amplitudes. A different off-shell kinematic condition specifies each of the half-off-shell amplitudes. These four off-shell kinematic conditions can be expressed as [6,7]

$$\begin{aligned} s_f + u_2 + t_2 &= 4m^2 - 2P_1 \cdot K, \\ s_i + u_1 + t_2 &= 4m^2 + 2P_1' \cdot K, \\ s_f + u_1 + t_1 &= 4m^2 - 2P_2 \cdot K, \\ s_i + u_2 + t_1 &= 4m^2 + 2P_2' \cdot K. \end{aligned} \tag{16}$$

These expressions define the off-shell kinematic conditions for those external processes in which a photon is emitted from the P_1, P_1', P_2, and P_2' legs, respectively. Equations (16) are said to define the off-shell kinematic conditions, because each equation involves an off-shell factor ($P_1 \cdot K$, $P_1' \cdot K$, $P_2 \cdot K$, or $P_2' \cdot K$) and because there exist three independent variables in each of the four equations. From these four off-shell kinematic conditions, two well-defined sets of on-shell conditions can be obtained [6].

1. The four on-shell conditions specifying the TuTts amplitude

The first set of on-shell conditions can be defined by introducing new variables s_{ij} $(i, j = 1, 2)$ of the form

$$s_{ij} + u_i + t_j = 4m^2, \tag{17}$$

where

$$\begin{aligned} s_{22} &= s_f + 2P_1 \cdot K, \\ s_{12} &= s_i - 2P_1' \cdot K, \\ s_{11} &= s_f + 2P_2 \cdot K, \\ s_{21} &= s_i - 2P_2' \cdot K. \end{aligned} \tag{18}$$

Because there are only two independent variables in a given set of (s_{ij}, u_i, t_j), four separate on-shell points $[(u_i, t_j), i, j = 1, 2$ or $(s_{ij}, t_j)]$ can be defined, and we can write

$$F_\alpha^e(u_i, t_j) = F_\alpha^e(s_{ij}, t_j). \tag{19}$$

Moreover, as shown in Ref. [6], four center-of-mass momenta $q_{\text{c.m.}}^{ij}$ and four center-of-mass angles $\theta_{\text{c.m.}}^{ij}$ can be obtained from the four given on-shell points (s_{ij}, t_j). In other words, $F_\alpha^e(s_{ij}, t_j)$ is evaluated at the set of $(q_{\text{c.m.}}^{ij}, \theta_{\text{c.m.}}^{ij})$,

$$F_\alpha^e(u_i, t_j) = F_\alpha^e(s_{ij}, t_j) = F_\alpha^e\big(q_{\text{c.m.}}^{ij}, \theta_{\text{c.m.}}^{ij}\big). \tag{20}$$

Thus, by imposing the on-shell conditions given by Eq. (17), $F_\alpha^e(u_i, t_j)$ can be treated as on-shell amplitudes. We emphasize that the on-shell conditions given by Eq. (17) are equivalent to the original four off-shell kinematic conditions specified by Eqs. (16). Therefore, the choice of the four separate on-shell points at which to evaluate the TuTts amplitude M_μ^{TuTts} is both natural and physical. Furthermore, because of such a choice, the amplitude M_μ^{TuTts} is free of any derivative of $F_\alpha^e(u_i, t_j)$ with respect to u and/or t. For the $pp\gamma$ process, an important advantage of using the amplitude M_μ^{TuTts} is that it retains most of the contributions from the κ_p-dependent terms [3]. In fact, these κ_p-dependent terms were shown to play a key role in $pp\gamma$ cross sections for the kinematic conditions reported in Ref. [3].

2. The single on-shell condition specifying the Low amplitude

The second set of on-shell conditions involves only a single equation, and it has been used in the Low amplitude. If we add the four off-shell kinematic conditions defined by Eqs. (16), we find

$$\bar{s} + \bar{u} + \bar{t} = 4m^2, \tag{21}$$

where

$$\begin{aligned} \bar{s} &= \tfrac{1}{2}(s_i + s_f), \\ \bar{u} &= \tfrac{1}{2}(u_1 + u_2), \\ \bar{t} &= \tfrac{1}{2}(t_1 + t_2). \end{aligned}$$

All four off-shell factors cancel precisely because of energy-momentum conservation and the condition $K_\mu K^\mu = 0$. Equation (21) defines a unique on-shell point, $(\bar{s}, \bar{t})$, and all F_α^e are to be evaluated at this common point for the Low amplitude. Because only a single on-shell point is used, each of the four half-off-shell external emission amplitudes must be expanded about $(\bar{s}, \bar{t})$ before the gauge invariance condition can be imposed to determine the corresponding internal amplitude. Therefore, the input for the Low amplitude M_μ^{Low} will be the on-shell amplitudes $F_\alpha^e(\bar{s}, \bar{t})$ and their derivatives evaluated at $(\bar{s}, \bar{t})$. This expansion about the special on-shell point $(\bar{s}, \bar{t})$ is standard in the Low procedure. As pointed out in Ref. [3], a serious drawback of using the Low procedure for the $pp\gamma$ process is that an essential part of the important contribution from the κ_p-dependent terms will be lost. To see this, let us compare the amplitude M_μ^{TuTts} with the Low amplitude M_μ^{Low}.

C. The relationship between M_μ^{TuTts} and M_μ^{Low}

The Low amplitude for both $pp\gamma$ and $np\gamma$ processes was first derived by Nyman [8]. The on-shell point defined in Nyman's original derivation was (ν, Δ), where $\nu = \bar{s} - 2m^2$ and $\Delta = 2m^2 - \bar{t}$. Here we use the on-shell point $(\bar{s}, \bar{t})$, which has been used by most other authors. The fact that the Low amplitude M_μ^{Low} for $pp\gamma$ and $np\gamma$ can be reproduced from the TuTts amplitude M_μ^{TuTts} was demonstrated in Ref. [3]. In order to show that the amplitude M_μ^{Low} (for all three $pp\gamma$, $np\gamma$, and $nn\gamma$ processes) can be obtained from the amplitude M_μ^{TuTts} given by Eq. (13), we must expand M_μ^{TuTts} about the on-shell point $(\bar{s}, \bar{t})$. Using the following expressions

$$\begin{aligned} s_{12} &= \bar{s} + (P_2' - P_1') \cdot K, \\ s_{22} &= \bar{s} + (P_1 - P_2) \cdot K, \\ s_{21} &= \bar{s} - (P_2' - P_1') \cdot K, \\ s_{11} &= \bar{s} - (P_1 - P_2) \cdot K, \\ t_1 &= \bar{t} - (P_2 - P_2') \cdot K, \\ t_2 &= \bar{t} + (P_2 - P_2') \cdot K, \end{aligned} \tag{22}$$

to expand $F_\alpha^e(u_i, t_j) = F_\alpha^e(s_{ij}, t_j)$ for $i, j = 1, 2$, we find

$$\begin{aligned} F_\alpha^e(u_1, t_2) &= F_\alpha^e(s_{12}, t_2) \\ &= F_\alpha^e(\bar{s}, \bar{t}) + \frac{\partial F_\alpha^e(\bar{s}, \bar{t})}{\partial \bar{s}}(P_2' - P_1') \cdot K \\ &\quad + \frac{\partial F_\alpha^e(\bar{s}, \bar{t})}{\partial \bar{t}}(P_2 - P_2') \cdot K, \end{aligned}$$

$$\begin{aligned}
F^e_\alpha(u_2, t_2) &= F^e_\alpha(s_{22}, t_2)\\
&= F^e_\alpha(\bar{s}, \bar{t}) + \frac{\partial F^e_\alpha(\bar{s}, \bar{t})}{\partial \bar{s}}(P_1 - P_2)\cdot K\\
&\quad + \frac{\partial F^e_\alpha(\bar{s}, \bar{t})}{\partial \bar{t}}(P_2 - P_2')\cdot K,\\
F^e_\alpha(u_2, t_1) &= F^e_\alpha(s_{21}, t_1)\\
&= F^e_\alpha(\bar{s}, \bar{t}) - \frac{\partial F^e_\alpha(\bar{s}, \bar{t})}{\partial \bar{s}}(P_2' - P_1')\cdot K\\
&\quad - \frac{\partial F^e_\alpha(\bar{s}, \bar{t})}{\partial \bar{t}}(P_2 - P_2')\cdot K,\\
F^e_\alpha(u_1, t_1) &= F^e_\alpha(s_{11}, t_1)\\
&= F^e_\alpha(\bar{s}, \bar{t}) - \frac{\partial F^e_\alpha(\bar{s}, \bar{t})}{\partial \bar{s}}(P_1 - P_2)\cdot K\\
&\quad - \frac{\partial F^e_\alpha(\bar{s}, \bar{t})}{\partial \bar{t}}(P_2 - P_2')\cdot K.
\end{aligned} \tag{23}$$

Substituting Eqs. (23) into Eq. (13), we obtain the following special soft-photon expansion:

$$M^{\rm TuTts}_\mu = M^{\rm Low}_\mu + M^{(3)}_\mu(K^1) + O_\mu(K^2), \tag{24}$$

where

$$\begin{aligned}
M^{\rm Low}_\mu &= M^{(1)}_\mu(K^{-1}; e) + M^{(2)}_\mu(K^0),\\
M^{(1)}_\mu(K^{-1}; e) &= \left(\frac{e_1 P'_{1\mu}}{P_1'\cdot K} - \frac{e_1 P_{1\mu}}{P_1\cdot K}\right.\\
&\qquad \left. + \frac{e_2 P'_{2\mu}}{P_2'\cdot K} - \frac{e_2 P_{2\mu}}{P_2\cdot K}\right) F(\bar{s}, \bar{t}),\\
F(\bar{s}, \bar{t}) &= \sum_{\alpha=1}^{5} F^e_\alpha(\bar{s}, \bar{t})\, U_\alpha(1)U^\alpha(2),\\
M^{(2)}_\mu(K^0) &= M^{\rm mag}_\mu(K^0) + M^{\rm ex}_\mu(K^0; e),\\
M^{\rm mag}_\mu(K^0) &= M^{\rm mag}_\mu(e) + M^{\rm mag}_\mu(\kappa),\\
M^{\rm mag}_\mu(e) &= \sum_{\alpha=1}^{5} F^e_\alpha(\bar{s}, \bar{t}) \left[\bar{u}(P_1') Z^{(1)}_{\mu\alpha}(e) u(P_1) U^\alpha(2)\right.\\
&\quad \left. +\ U^\alpha(1)\bar{u}(P_2') Z^{(2)}_{\mu\alpha}(e) u(P_2)\right],\\
M^{\rm mag}_\mu(\kappa) &= \sum_{\alpha=1}^{5} F^e_\alpha(\bar{s}, \bar{t}) \left[\bar{u}(P_1') Z^{(1)}_{\mu\alpha}(\kappa) u(P_1) U^\alpha(2)\right.\\
&\quad \left. +\ U^\alpha(1)\bar{u}(P_2') Z^{(2)}_{\mu\alpha}(\kappa) u(P_2)\right],\\
M^{\rm ex}_\mu(K^0; e) &= \sum_{\alpha=1}^{5} \frac{\partial F^e_\alpha(\bar{s}, \bar{t})}{\partial \bar{s}}\Bigg[(P_2' - P_1')\cdot K\\
&\quad \times \left(\frac{e_1 P'_{1\mu}}{P_1'\cdot K} - \frac{e_2 P'_{2\mu}}{P_2'\cdot K}\right) - (P_1 - P_2)\cdot K\\
&\quad \times \left(\frac{e_1 P_{1\mu}}{P_1\cdot K} - \frac{e_2 P_{2\mu}}{P_2\cdot K}\right) - 2(P_1 - P_2')\cdot K\\
&\quad \times (V_{y\mu} - V_{x\mu})\Bigg] U_\alpha(1)U^\alpha(2)\\
&\quad + \sum_{\alpha=1}^{5} \frac{\partial F^e_\alpha(\bar{s}, \bar{t})}{\partial \bar{t}}\Bigg[(P_2 - P_2')\cdot K\\
&\quad \times \left(\frac{e_1 P'_{1\mu}}{P_1'\cdot K} - \frac{e_1 P_{1\mu}}{P_1\cdot K} + \frac{e_2 P_{2\mu}}{P_2\cdot K} - \frac{e_2 P'_{2\mu}}{P_2'\cdot K}\right)\Bigg]\\
&\quad \times U_\alpha(1)U^\alpha(2),\\
M^{(3)}_\mu(K^1) &= M^{(3)}_\mu(e) + M^{(3)}_\mu(\kappa),\\
M^{(3)}_\mu(e) &= \sum_{\alpha=1}^{5} \frac{\partial F^e_\alpha(\bar{s}, \bar{t})}{\partial \bar{s}} \left[U^\alpha(1)\bar{u}(P_2')\widetilde{Z}^{(2)}_{\mu\alpha}(e) u(P_2)\right.\\
&\quad \left. - \bar{u}(P_1')\widetilde{Z}^{(1)}_{\mu\alpha}(e) u(P_1) U^\alpha(2)\right]\\
&\quad + \sum_{\alpha=1}^{5} \frac{\partial F^e_\alpha(\bar{s}, \bar{t})}{\partial \bar{t}}(P_2 - P_2')\cdot K\\
&\quad \times \left[\bar{u}(P_1') Z^{(1)}_{\mu\alpha}(e) u(P_1) U^\alpha(2)\right.\\
&\quad \left. - U^\alpha(1)\bar{u}(P_2') Z^{(2)}_{\mu\alpha}(e) u(P_2)\right],\\
M^{(3)}_\mu(\kappa) &= \sum_{\alpha=1}^{5} \frac{\partial F^e_\alpha(\bar{s}, \bar{t})}{\partial \bar{s}} \left[U^\alpha(1)\bar{u}(P_2')\widetilde{Z}^{(2)}_{\mu\alpha}(\kappa) u(P_2)\right.\\
&\quad \left. - \bar{u}(P_1')\widetilde{Z}^{(1)}_{\mu\alpha}(\kappa) u(P_1) U^\alpha(2)\right]\\
&\quad + \sum_{\alpha=1}^{5} \frac{\partial F^e_\alpha(\bar{s}, \bar{t})}{\partial \bar{t}}(P_2 - P_2')\cdot K\\
&\quad \times \left[\bar{u}(P_1') Z^{(1)}_{\mu\alpha}(\kappa) u(P_1) U^\alpha(2)\right.\\
&\quad \left. - U^\alpha(1)\bar{u}(P_2') Z^{(2)}_{\mu\alpha}(\kappa) u(P_2)\right].
\end{aligned} \tag{25}$$

Here we have defined ($j = 1, 2$)

$$\begin{aligned}
U^\alpha(j) &= \bar{u}(P_j')\lambda^\alpha u(P_j),\\
U_\alpha(j) &= \bar{u}(P_j')\lambda_\alpha u(P_j),\\
Z^{(j)}_{\mu\alpha}(e) &= \frac{R^{P_j'}_{j\mu}(e)}{P_j'\cdot K}\lambda_\alpha - \lambda_\alpha \frac{R^{P_j}_{j\mu}(e)}{P_j\cdot K},\\
Z^{(j)}_{\mu\alpha}(\kappa) &= \frac{R^{P_j'}_{j\mu}(\kappa)}{P_j'\cdot K}\lambda_\alpha - \lambda_\alpha \frac{R^{P_j}_{j\mu}(\kappa)}{P_j\cdot K},\\
\widetilde{Z}^{(j)}_{\mu\alpha}(e) &= (P_1' - P_2')\cdot K \frac{R^{P_j'}_{j\mu}(e)}{P_j'\cdot K}\lambda_\alpha\\
&\quad + (P_1 - P_2)\cdot K \lambda_\alpha \frac{R^{P_j}_{j\mu}(e)}{P_j\cdot K},\\
\widetilde{Z}^{(j)}_{\mu\alpha}(\kappa) &= (P_1' - P_2')\cdot K \frac{R^{P_j'}_{j\mu}(\kappa)}{P_j'\cdot K}\lambda_\alpha\\
&\quad + (P_1 - P_2)\cdot K \lambda_\alpha \frac{R^{P_j}_{j\mu}(\kappa)}{P_j\cdot K},
\end{aligned} \tag{26}$$

along with the modified vertex functions

$$\begin{aligned} R^{P'_j}_{j\mu}(e) &= R^{P_j}_{j\mu}(e), \\ &= \frac{e_j}{4}[\gamma_\mu, \not{K}], \\ R^{P'_j}_{j\mu}(\kappa) &= \frac{\kappa_j}{8m}\{[\gamma_\mu, \not{K}], \not{P}'_j\}, \\ R^{P_j}_{j\mu}(\kappa) &= \frac{\kappa_j}{8m}\{[\gamma_\mu, \not{K}], \not{P}_j\}. \end{aligned}$$

In Eqs. (24) and (25), $M^{(1)}_\mu(K^{-1};e)$, $M^{(2)}_\mu(K^0)$, and $M^{(3)}_\mu(K^1)$ are the terms of order K^{-1}, K^0, and K^1, respectively, in the soft-photon expansion. $M^{(1)}_\mu(K^{-1};e)$, which involves only the charge contribution, is the leading external amplitude. $F(\bar{s},\bar{t})$ is the NN (pp, np, nn) elastic scattering amplitude. $M^{\text{ex}}_\mu(K^0)$ includes the external terms of order K^0 and the internal exchange current (gauge) contribution of the same order. Both $M^{\text{mag}}_\mu(K^0)$, of order K^0, and $M^{(3)}_\mu(K^1)$, of order K^1, which belong to the external amplitude contribution, are functions of the charges of the nucleons and the anomalous magnetic moments κ_p for the proton and κ_n for the neutron.

The expansion given by Eq. (24) demonstrates that the TuTts amplitude M^{TuTts}_μ is identical to the Low amplitude M^{Low}_μ through order K^0 in the soft-photon expansion. Moreover, Eq. (24) shows that the amplitude M^{TuTts}_μ includes $M^{(3)}_\mu(K^1)$, which cannot be obtained if the Low procedure is used. It is interesting to note that the expression for $M^{(3)}_\mu(K^1)$ is the same for all three of the (different) $NN\gamma$ processes, $pp\gamma$, $np\gamma$, and $nn\gamma$. As was pointed out in Ref. [3], the amplitudes M^{TuTts}_μ and M^{Low}_μ yield very similar $np\gamma$ cross sections, but they predict quite different $pp\gamma$ cross sections. Moreover, in the $pp\gamma$ case the amplitude M^{TuTts}_μ is a better soft-photon approximation than is the amplitude M^{Low}_μ. It was concluded in Ref. [3] that the amplitude M^{TuTts}_μ describes the $pp\gamma$ better than does the amplitude M^{Low}_μ, primarily because the κ_p contribution is so significant that the additional term $M^{(3)}_\mu(K^1)$ cannot be neglected. In contrast, in the $np\gamma$ case, the κ_p and κ_n contributions are so small that the $M^{\text{mag}}_\mu(K^0)$ and $M^{(3)}_\mu(K^1)$ terms are essentially negligible. Therefore, the M^{TuTts}_μ and M^{Low}_μ amplitudes are approximately equivalent, and they predict quantitatively similar $np\gamma$ cross-sections. These conclusions [3] were drawn from the comparison of cross-section calculations using M^{TuTts}_μ as given by Eq. (13) and $M^{\text{Low}}_\mu[= M^{(1)}_\mu(K^{-1};e) + M^{(2)}_\mu(K^0)]$ given by Eq. (25) with and without the contribution from κ_p and κ_n. In other words, the contribution coming from $M^{(3)}_\mu(K^1)$ has not been investigated directly; this can be done through the use of the approximation $M^{\text{TuTts}}_\mu \simeq M^{\text{Low}}_\mu + M^{(3)}_\mu(K^1)$ given by Eq. (24). Because the investigation of the anomalous magnetic moment effect in $NN\gamma$ cross sections is the primary focus of this work, we must carefully study the contributions from $M^{(3)}_\mu(K^1)$. Therefore, we define the following amplitudes:

$$\begin{aligned} M^{\text{TuTts}}_{(1)\mu} &= M^{\text{Low}}_\mu + M^{(3)}_\mu(K^1), \\ &= M^{\text{Low}}_\mu + M^{(3)}_\mu(e) + M^{(3)}_\mu(\kappa), \end{aligned} \tag{27}$$

$$M^{\text{TuTts}}_{(2)\mu} = M^{\text{Low}}_\mu + M^{(3)}_\mu(\kappa), \tag{28}$$

$$M^{\text{TuTts}}_{(3)\mu} = M^{\text{Low}}_\mu + M^{(3)}_\mu(e). \tag{29}$$

These amplitudes can be used to calculate $NN\gamma$ cross sections. In order to demonstrate that the cross sections calculated using these amplitudes can be used to investigate the contributions from $M^{(3)}_\mu(K^1)$, we have applied these amplitudes to the $pp\gamma$ process, because the $M^{(3)}_\mu(K^1)$ contribution to $pp\gamma$ cross sections is important. Furthermore, the best way to check and to understand our $nn\gamma$ results is to compare the $nn\gamma$ and $pp\gamma$ cross sections using the following special $pp\gamma$ amplitude:

$$\begin{aligned} M^{\text{TuTts}}_{(4)\mu} &= \left[M^{\text{TuTts}}_\mu(pp\gamma)\right]_{e=0} \\ &= M^{\text{mag}}_\mu(\kappa_p) + M^{(3)}_\mu(\kappa_p) + \left[O^{(p)}_\mu(K^2)\right]_{e=0}. \end{aligned} \tag{30}$$

In other words, $M^{\text{TuTts}}_{(4)\mu}$ is obtained from M^{TuTts}_μ by setting the proton charge to be zero. Moreover, we should point out that the M^{TuTts}_μ amplitude for the $nn\gamma$ process has the following expansion:

$$M^{\text{TuTts}}_\mu(nn\gamma) = M^{\text{mag}}_\mu(\kappa_n) + M^{(3)}_\mu(\kappa_n) + O^{(n)}_\mu(K^2), \tag{31}$$

which has a form quite similar to that for $M^{\text{TuTts}}_{(4)\mu}$ given by Eq. (30). The major difference between $M^{\text{TuTts}}_{(4)\mu}$ and $M^{\text{TuTts}}_\mu(nn\gamma)$ is that the amplitudes M^{mag}_μ and $M^{(3)}_\mu$ in Eq. (30) are evaluated for κ_p while those in Eq. (31) are evaluated for κ_n.

Altogether we have defined a set of 12 amplitudes:

$$\begin{aligned} M_\mu \equiv \big\{&M^{\text{TuTts}}_\mu, M^{\text{Low}}_\mu, M^{(1)}_\mu(K^{-1};e), M^{\text{mag}}_\mu(e), \\ &M^{\text{mag}}_\mu(\kappa), M^{\text{ex}}_\mu(K^0;e), M^{(3)}_\mu(e), M^{(3)}_\mu(\kappa), \\ &M^{\text{TuTts}}_{(1)\mu}, M^{\text{TuTts}}_{(2)\mu}, M^{\text{TuTts}}_{(3)\mu}, M^{\text{TuTts}}_{(4)\mu}\big\}. \end{aligned} \tag{32}$$

It is easily verified that each amplitude in M_μ separately satisfies the gauge condition $M_\mu K^\mu = 0$. In other words, M_μ represents a set of conserved currents. Because the gauge condition is satisfied, the following relation can be established for each amplitude in M_μ:

$$\sum_{\text{pol}}[(\epsilon^\mu M_\mu)^\dagger(\epsilon^\nu M_\nu)] = -M^\dagger_\mu M^\mu \equiv -|M_\mu|^2. \tag{33}$$

Here, ϵ^μ is the photon polarization vector and $\sum$ signifies the summation over polarization. Thus, we have shown that the cross section calculated from the amplitude M_μ is directly proportional to $|M_\mu|^2 \equiv M^\dagger_\mu M_\mu$. We can also find that the amplitudes $\{M^{\text{TuTts}}_\mu, M^{\text{Low}}_\mu, M^{\text{TuTts}}_{(1)\mu}, M^{\text{TuTts}}_{(2)\mu}, M^{\text{TuTts}}_{(3)\mu}, M^{\text{TuTts}}_{(4)\mu}\}$ have been expanded in terms of the six basic amplitudes $\{M^{(1)}_\mu(K^{-1};e), M^{\text{mag}}_\mu(e), M^{\text{mag}}_\mu(\kappa), M^{\text{ex}}_\mu(K^0;e), M^{(3)}_\mu(e), M^{(3)}_\mu(\kappa)\}$. These latter six basic amplitudes play an important role in the analysis of our results, as discussed in the following section.

III. RESULTS AND DISCUSSION

We have utilized the M^{TuTts}_μ [Eq. (13)] and M^{Low}_μ [Eq. (25)] amplitudes to calculate coplanar $NN\gamma$ cross sections $d^3\sigma/d\Omega_1 d\Omega_2 d\psi_\gamma$ as functions of the photon angle ψ_γ for several laboratory nucleon bombarding energies above 150 MeV and for laboratory scattering angles lying between 8° and 40°. In each of these calculations, we used two different sets

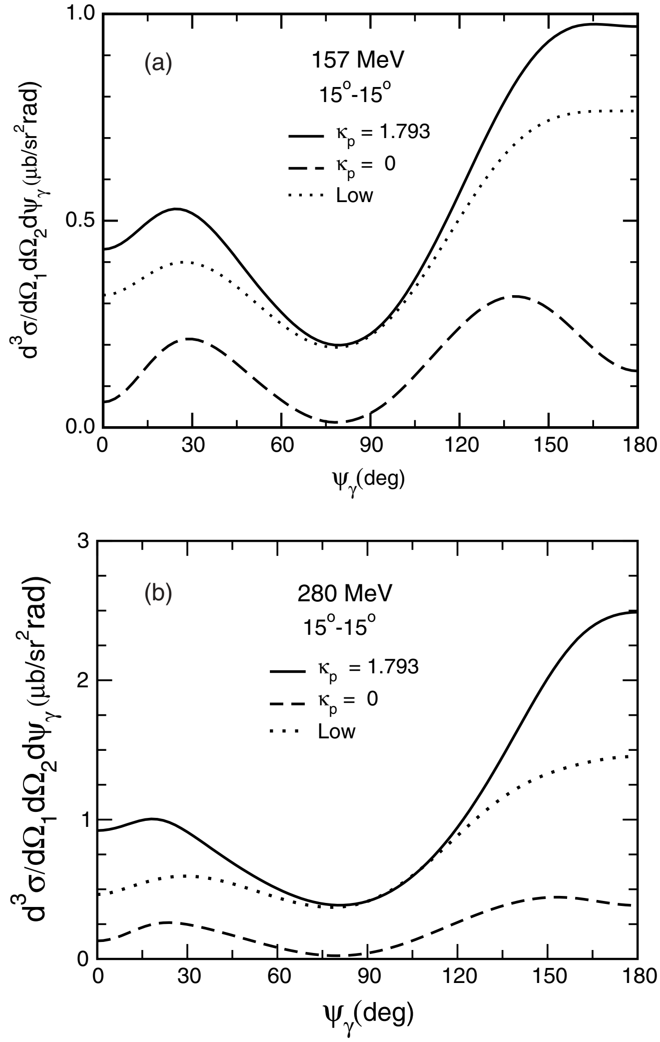

FIG. 1. Coplanar $pp\gamma$ cross sections as a function of the photon angle ψ_γ at (a) 157 MeV and (b) 280 MeV for the symmetric proton scattering angle configuration $\theta_1 = \theta_2 = 15^\circ$. The solid curve was calculated using $M_\mu^{\rm TuTts}$ with $\kappa_p = 1.793$; the dashed curve was calculated using the same amplitude $M_\mu^{\rm TuTts}$ but with $\kappa_p = 0$; the dotted curve was calculated using $M_\mu^{\rm Low}$ with $\kappa_p = 1.793$.

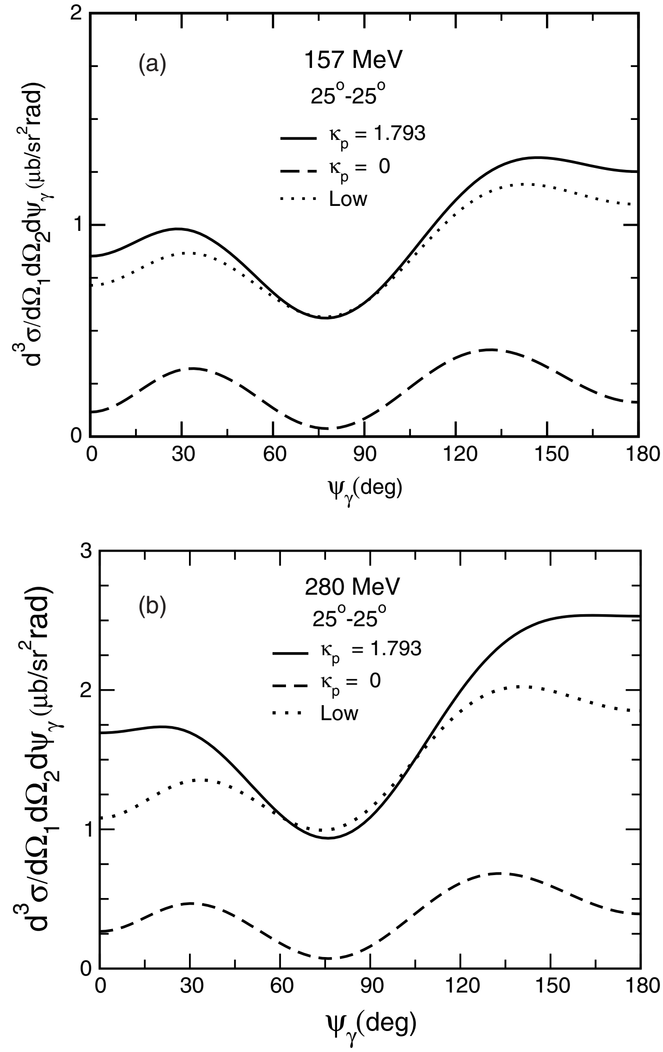

FIG. 2. Same as Fig. 1, but for $\theta_1 = \theta_2 = 25^\circ$.

of values for the nucleon anomalous magnetic moments: (1) corresponding to the physical values of $\kappa_p = 1.793$ and $\kappa_n = -1.913$ and (2) corresponding to zero anomalous magnetic moment contributions $\kappa_p = \kappa_n = 0$. Results for these two sets of anomalous magnetic moment values were compared to investigate anomalous magnetic moment effects. Moreover, in our investigation of the contribution from $M_\mu^{(3)}(K^1)$ and the comparison between $nn\gamma$ and $pp\gamma$, we have also used four additional amplitudes, $M_{(1)\mu}^{\rm TuTts}$, $M_{(2)\mu}^{\rm TuTts}$, $M_{(3)\mu}^{\rm TuTts}$, and $M_{(4)\mu}^{\rm TuTts}$ [Eqs. (27)–(30)] in calculating $pp\gamma$ cross sections. To evaluate $F_\alpha^e(q_{\rm c.m.}^{ij}, \theta_{\rm c.m.}^{ij})$, we used the pp and np phase shifts and mixing parameters from the Nijmegen partial-wave analysis [9,10]. For the nn system, the phase shifts were assumed to be equal to the corresponding pp ones, with the Coulomb interaction set to zero.

A. $pp\gamma$

In Figs. 1–4, we present coplanar $pp\gamma$ cross sections at 157 MeV [Figs. 1(a)–4(a)] and 280 MeV [Figs. 1(b)–4(b)] for four symmetric proton scattering angle pairs, $\theta_1 = \theta_2 = 15^\circ, 25^\circ, 35^\circ,$ and 40°. In each of these figures, we show three different curves: The solid curve corresponds to a cross section calculated using the $M_\mu^{\rm TuTts}$ amplitude with the value of $\kappa_p = 1.793$; the dotted curve corresponds to a cross section calculated using the $M_\mu^{\rm Low}$ amplitude also with the value of $\kappa_p = 1.793$; the dashed curve corresponds to a cross section calculated using the $M_\mu^{\rm TuTts}$ amplitude but with the value of $\kappa_p = 0$. Figures 1–4 are arranged according to the size of the scattering angle θ ($\theta = \theta_1 = \theta_2 = 15^\circ, 25^\circ, 25^\circ, 40^\circ$) and the magnitude of the bombarding energy E_i (157 and 280 MeV). Several interesting features of these results and their physical implications can be summarized as follows:

(i) First we highlight some important points regarding the curves. (a) Both the solid curve and the dotted curve depend upon the contribution from the proton charge, the

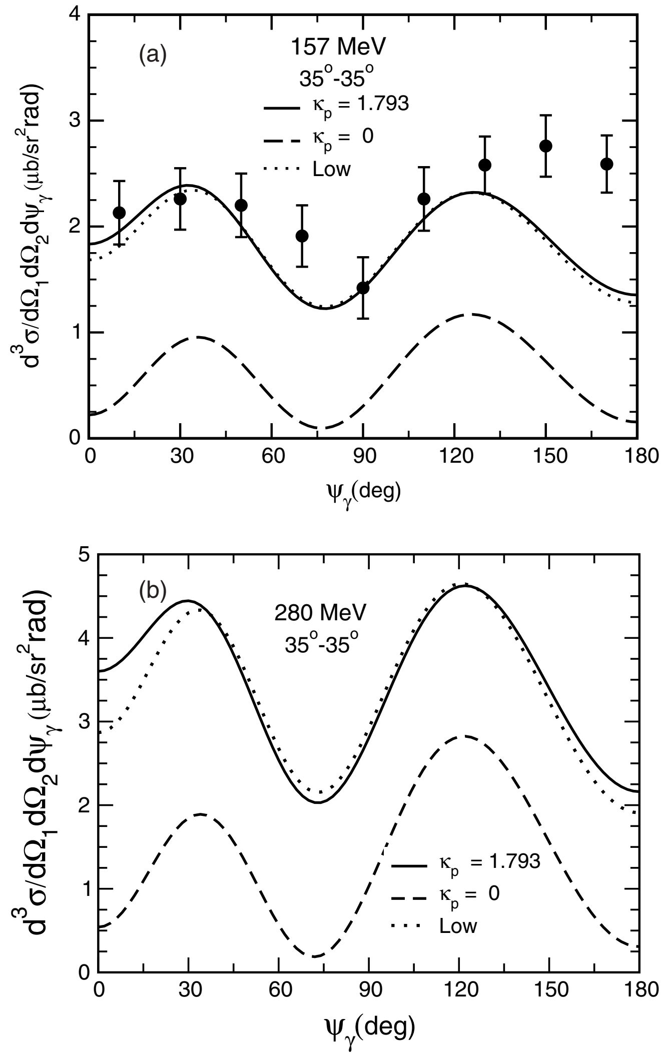

FIG. 3. Same as Fig. 1, but for $\theta_1 = \theta_2 = 35^\circ$. The data at 157 MeV are from Ref. [11].

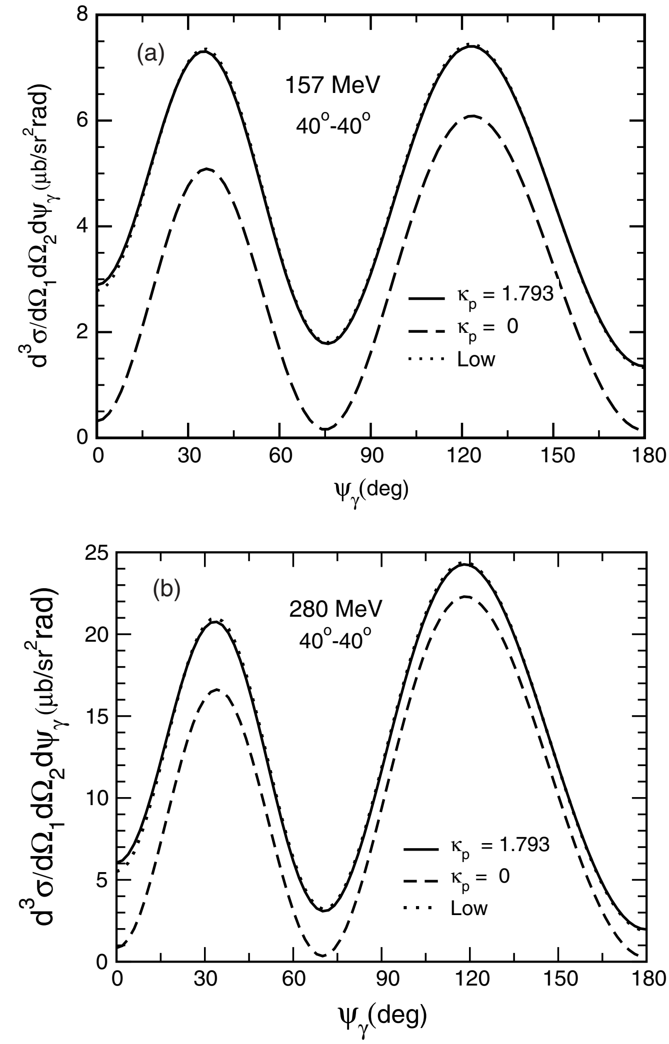

FIG. 4. Same as Fig. 1, but for $\theta_1 = \theta_2 = 40^\circ$.

Dirac magnetic moment of the proton, and the proton anomalous magnetic moment κ_p, while the dashed curve depends only upon the contributions from the proton charge and the Dirac magnetic moment of the proton (κ_p having been set to zero in the calculation). (b) The $pp\gamma$ cross section $\sigma_{pp\gamma}$ has the soft-photon expansion

$$\begin{aligned}\sigma_{pp\gamma} &= A/K + B + CK + \cdots \\ &\simeq A/K + B \\ &\equiv \sigma_{pp\gamma}^{\mathrm{SPA}},\end{aligned}$$

where $\sigma_{pp\gamma}^{\mathrm{SPA}}$ is the soft-photon approximation. The coefficient A depends on the charge contribution and B depends on the contributions from the charge, the Dirac moment, and κ_p. The leading term of the soft-photon approximation is A/K. However, because there are two identical protons in the scattering process, certain cancellation occurs within the leading term. It is this cancellation which greatly reduces the contribution to $\sigma_{pp\gamma}^{\mathrm{SPA}}$ from the leading term when the soft-photon approximation is used to represent the $pp\gamma$ cross section. In this case, the B term is more important than the A/K term for the hard-photon case. In fact, the $1/K$ dependence of the leading term means that the cross section diverges when K tends to zero in the soft-photon limit. It is well known that K will correspond to a hard photon for small scattering angle θ, whereas K will correspond to a soft photon for large angle θ. Moreover, the statement "K tends to zero in the soft-photon limit" is equivalent to the statement "θ tends to 45° in the elastic limit." With these caveats, we can understand why cross sections corresponding to the dashed curves are small for small angles θ and why these cross sections increase as θ increases. In fact, the leading term dominates the cross section for the case with $\theta = 40^\circ$ (near the elastic limit). (c) Without the contribution from κ_p the cross section will have a standard quadrupole distribution. The dashed curves shown in Figs. 1–4 are typical examples. A significant contribution from κ_p can modify the angular distribution from the quadrupole shape, as one can see from the solid and dotted curves shown in Figs. 1 and 2.

(ii) The primary purpose of this investigation is to understand the effect of the anomalous magnetic moment κ_p. If we compare the solid curve with the dashed curve in each of the eight panels shown in Figs. 1–4, then we can see the difference in cross section between these two calculations as a function of θ and ψ_γ for $E_i = 157$ and 280 MeV. Let us define $\Delta\sigma_{\text{mag}}(\theta, \psi_\gamma; E_i)$ to be the difference in the $pp\gamma$ cross section between the solid curve and the dashed curve for a given set of kinematic variables $(\theta, \psi_\gamma; E_i)$. This $\Delta\sigma_{\text{mag}}(\theta, \psi_\gamma; E_i)$ tells one much about the effect of κ_p. This can be seen from the following analysis. The amplitude M_μ^{TuTts}, defined by Eq. (24), can also be written in the form

$$M_\mu^{\text{TuTts}} = M_{(4)\mu}^{\text{TuTts}} + M_{(5)\mu}^{\text{TuTts}}, \tag{34}$$

where $M_{(4)\mu}^{\text{TuTts}}$ is given by Eq. (30) and $M_{(5)\mu}^{\text{TuTts}}$ can be expressed as

$$\begin{aligned} M_{(5)\mu}^{\text{TuTts}} &\equiv \left(M_\mu^{\text{TuTts}}\right)_{\kappa_p=0} \\ &= M_\mu^{(1)}(K^{-1}; e) + M_\mu^{\text{mag}}(e) + M_\mu^{\text{ex}}(K^0; e) \\ &\quad + M_\mu^3(e) + [O_\mu(K^2)]_{\kappa_p=0}. \end{aligned} \tag{35}$$

Equation (34) leads to

$$\left|M_\mu^{\text{TuTts}}\right|^2 = \left|M_{(5)\mu}^{\text{TuTts}}\right|^2 + \Delta_{\text{mag}}, \tag{36}$$

where

$$\begin{aligned} \Delta_{\text{mag}} = &\left|M_{(4)\mu}^{\text{TuTts}}\right|^2 + \left(M_{(4)\mu}^{\text{TuTts}}\right)^\dagger \left(M_{(5)}^{\text{TuTts}\mu}\right) \\ &+ \left(M_{(5)\mu}^{\text{TuTts}}\right)^\dagger \left(M_{(4)}^{\text{TuTts}\mu}\right). \end{aligned} \tag{37}$$

Because the solid curve is directly proportional to $|M_\mu^{\text{TuTts}}|^2$ and the dashed curve is directly proportional to $|M_{(5)\mu}^{\text{TuTts}}|^2$, $\Delta\sigma_{\text{mag}}(\theta, \psi_\gamma; E_i)$ must be directly proportional to Δ_{mag}. We emphasize two important cases: (a) For the case with small scattering angles ($\theta \leqslant 25^\circ$), the contribution from $|M_{(5)\mu}^{\text{TuTts}}|^2$ (the dashed curve) is generally small while the Δ_{mag} term is much greater than the $|M_{(5)\mu}^{\text{TuTts}}|^2$ term. Moreover, the major contribution to the Δ_{mag} term comes from the amplitude $M_{(4)\mu}^{\text{TuTts}}$, which is proportional to κ_p. Therefore, the amplitude $M_{(4)\mu}^{\text{TuTts}}$ determines most of Δ_{mag} (or $|M_\mu^{\text{TuTts}}|^2$), and hence the contribution from κ_p will dominate the $pp\gamma$ cross section in this case. (b) For the case with θ approaching 45° (the elastic limit), $M_\mu^{(1)}(K^{-1}; e)$ in the expression for $M_{(5)\mu}^{\text{TuTts}}$ will become the dominant amplitude. In this case, $|M_{(5)\mu}^{\text{TuTts}}|^2$ will be much greater than Δ_{mag}, and $\Delta\sigma_{\text{mag}}(\theta, \psi_\gamma; E_i)$ will become very small. Hence, the κ_p contribution will be reduced to a negligible one. In short, the contribution of κ_p will reach its maximum (have its most significant effect) when θ tends to zero, and it will reach its minimum (having an essentially negligible effect) as θ approaches 45°. In addition, we observe that $\Delta\sigma_{\text{mag}}(\theta, \psi_\gamma; E_i)$ varies as a function of E_i, which implies that the effect of κ_p also depends upon E_i. However, the κ_p effect is clearly a more sensitive function of θ than of E_i.

(iii) Understanding the cross-section difference between the calculation using the M_μ^{TuTts} amplitude and that using the M_μ^{Low} amplitude is another important goal of this investigation. The analytic expression for the relationship between the two amplitudes is given by Eq. (24). In order to quantitatively explore the difference between the two cross sections, let us define $\Delta\sigma_{\text{amp}}(\theta, \psi_\gamma; E_i)$ to be the difference in cross section between the solid curve and the dotted curve as a function of θ and ψ_γ for $E_i = 157$ and 280 MeV. From Eq. (24) we obtain the following relationship between $|M_\mu^{\text{TuTts}}|^2$ and $|M_\mu^{\text{Low}}|^2$ for $pp\gamma$:

$$\left|M_\mu^{\text{TuTts}}\right|^2 = \left|M_\mu^{\text{Low}}\right|^2 + \Delta_{\text{amp}}, \tag{38}$$

where

$$\begin{aligned} \Delta_{\text{amp}} = &\left(M_\mu^{\text{Low}}\right)^\dagger [M^{(3)\mu}(K^1) + O^\mu(K^2)] \\ &+ \left[M_\mu^{(3)}(K^1) + O_\mu(K^2)\right]^\dagger M^{\text{Low}\mu} \\ &+ \left|M_\mu^{(3)}(K^1) + O_\mu(K^2)\right|^2. \end{aligned} \tag{39}$$

It should be clear that the solid curve is directly proportional to $|M_\mu^{\text{TuTts}}|^2$, that the dotted curve is directly proportional to $|M_\mu^{\text{Low}}|^2$, and that $\Delta\sigma_{\text{amp}}(\theta, \psi_\gamma; E_i)$ is directly proportional to Δ_{amp}. For small θ ($\theta \leqslant 25^\circ$), $\Delta\sigma_{\text{amp}}(\theta, \psi_\gamma; E_i)$ exhibits a minimum for angles ψ_γ in the region $65^\circ \leqslant \psi_\gamma \leqslant 90^\circ$, depending upon the specific values of θ and E_i. Around this minimum, the value of $\Delta\sigma_{\text{amp}}(\theta, \psi_\gamma; E_i)$ is nearly zero. This means that Δ_{amp} must also be nearly zero around the minimum, and we have

$$\left|M_\mu^{\text{TuTts}}\right|^2 \simeq \left|M_\mu^{\text{Low}}\right|^2. \tag{40}$$

Equation (40) implies that

$$M_\mu^{\text{TuTts}} \simeq M_\mu^{\text{Low}}. \tag{41}$$

Therefore, the contribution from $M_\mu^{(3)}(K^1)$ and higher-order terms $O_\mu(K^2)$ is negligible around the minimum, which is nearly zero. $\Delta\sigma_{\text{amp}}(\theta, \psi_\gamma; E_i)$ increases from the minimum to two separate maxima, a large one at $\psi_\gamma = 180^\circ$ and a smaller one at $\psi_\gamma = 0^\circ$. The magnitude of each maximum depends upon both θ and E_i. The magnitudes increase as θ decreases and increase as E_i increases. Equation (39) suggests that the values of $\Delta\sigma_{\text{amp}}(\theta, \psi_\gamma; E_i)$ arise primarily from the contribution of $M_\mu^{(3)}(K^1)$ and $O_\mu(K^2)$. As will be demonstrated in Fig. 5, the important contribution comes from the amplitude $M_\mu^{(3)}(K^1)$ for most photon angles ψ_γ. The contribution from higher-order terms $O_\mu(K^2)$ may be significant for ψ_γ near 0° and 180° in some cases. Therefore, our results imply that the contribution from $M_\mu^{(3)}(K^1; \kappa_p)$ is significant for those $pp\gamma$ cases with small scattering angles ($\theta \leqslant 25^\circ$). These findings explain why the Low amplitude, which does not include $M_\mu^{(3)}(K^1; \kappa_p)$ and $O_\mu(K^2)$, fails to describe much of the KVI data [12]. On the other hand, for those cases with a large scattering angle θ close to the elastic limit ($\theta \geqslant 40^\circ$), the value of $\Delta\sigma_{\text{amp}}(\theta, \psi_\gamma; E_i)$ is negligibly small for the entire range of ψ_γ. Thus, the M_μ^{TuTts} and M_μ^{Low} amplitudes are approximately equivalent in that region, and the two amplitudes predict quantitatively similar $pp\gamma$ cross

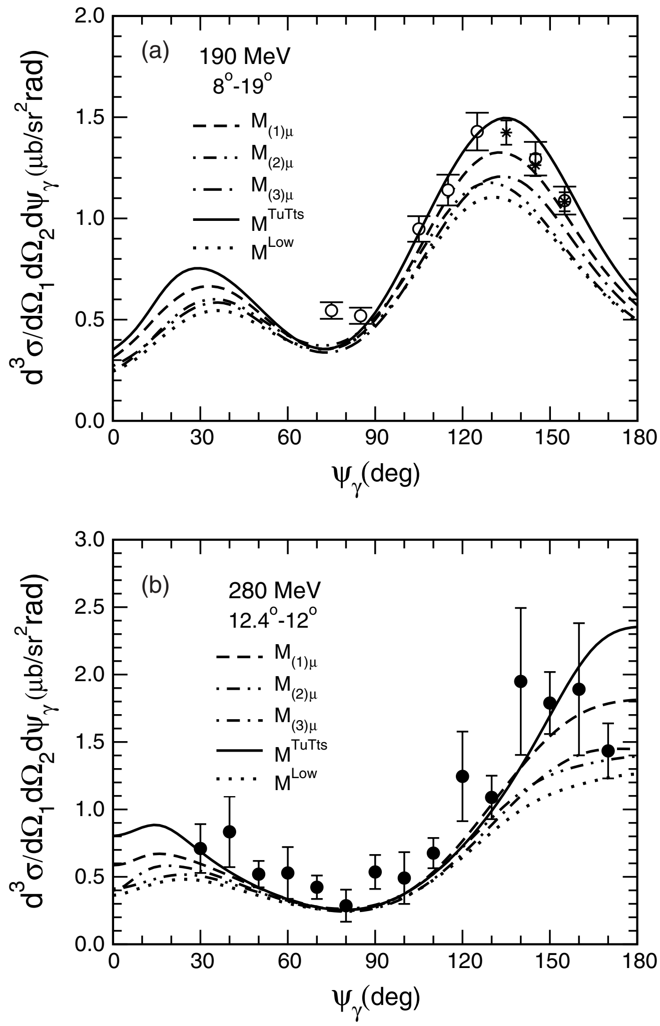

FIG. 5. Coplanar $pp\gamma$ cross sections as a function of the photon angle ψ_γ at (a) 190 MeV for the proton scattering angles $(\theta_1, \theta_2) = (8^\circ, 19^\circ)$; data from Ref. [12]; (b) at 280 MeV for $(\theta_1, \theta_2) = (12.4^\circ, 12^\circ)$; data from Ref. [13]. The five curves were calculated using the amplitudes shown in the symbols key.

sections. This implies that $M_\mu^{(3)}(K^1; \kappa_p)$ and all higher-order amplitudes are completely negligible for $pp\gamma$ with scattering angles $\theta \geqslant 40^\circ$.

(iv) The observant reader will see that all three curves have a minimum located at about the same value of ψ_γ in the region $65^\circ \leqslant \psi_\gamma \leqslant 90^\circ$. The solid and dotted curves give about the same cross sections in the vicinity of this minimum (i.e., $\Delta\sigma_{\text{amp}}(\theta, \psi_\gamma; E_i) \simeq 0$ around the minimum). As noted above, this implies that the contribution from the amplitude $M_\mu^{(3)}(K^1; \kappa_p)$ (and higher-order amplitudes) is negligible in this region. In contrast, the dashed curve has an almost negligible cross section around this minimum. This implies that the contribution from the amplitude $M_{(5)\mu}^{\text{TuTts}}$ is extremely small (essentially negligible). Therefore, comparing the solid curve (or the dotted curve) with the dashed curve, we can demonstrate that the contribution from the amplitude $M_\mu^{\text{mag}}(\kappa_p)$ [see Eq. (25)] should dominate the $pp\gamma$ cross sections in the vicinity of the minimum.

In Fig. 5, we present coplanar $pp\gamma$ cross sections at 190 MeV for proton angles $(\theta_1, \theta_2) = (8^\circ, 19^\circ)$ [Fig. 5(a)] and at 280 MeV for $(\theta_1, \theta_2) = (12.4^\circ, 12^\circ)$ [Fig. 5(b)]. The five different curves in these two figures correspond to calculations using the amplitudes M_μ^{TuTts}, $M_{(1)\mu}^{\text{TuTts}}$, $M_{(2)\mu}^{\text{TuTts}}$, $M_{(3)\mu}^{\text{TuTts}}$, and M_μ^{Low} (see symbols key in figure). These calculations illustrate several interesting and important results. We discuss some of them here.

(a) A primary purpose of these calculations is to investigate the contributions of the amplitudes $M_\mu^{(3)}(K^1)$, $M_\mu^{(3)}(e)$, and $M_\mu^{(3)}(\kappa_p)$. The most direct way to investigate the effect of the amplitude $M_\mu^{(3)}(K^1)$ is to compare the dashed curves generated using the amplitude $M_{(1)\mu}^{\text{TuTts}}$ with the dotted curves generated using the amplitude M_μ^{Low}. To understand this point, consider the following equation:

$$M_{(1)\mu}^{\text{TuTts}} = M_\mu^{\text{Low}} + M_\mu^{(3)}(K^1), \tag{42}$$

which leads to

$$\left|M_{(1)\mu}^{\text{TuTts}}\right|^2 = \left|M_\mu^{\text{Low}}\right|^2 + \Delta_1, \tag{43}$$

where

$$\Delta_1 = \left(M_\mu^{\text{Low}}\right)^\dagger M^{(3)\mu}(K^1) + [M^{(3)\mu}(K^1)]^\dagger M_\mu^{\text{Low}} + \left|M_\mu^{(3)}(K^1)\right|^2. \tag{44}$$

Equation (43) shows that the difference between the dashed and dotted curves is directly proportional to Δ_1, which depends upon $M_\mu^{(3)}(K^1)$, as exhibited in Eq. (44). The results shown in Fig. 5 demonstrate that the contribution from $M_\mu^{(3)}(K^1)$ is indeed quite significant in $pp\gamma$, because a large difference can be observed in Fig. 5 between the dashed and dotted curves for most photon angles ψ_γ.

(b) If we compare the solid curve generated using the amplitude M_μ^{TuTts} with the dashed curve, we can see the contribution from the higher-order terms $O_\mu(K^2)$. At 280 MeV, for example, the two curves are almost coincident in the region $40^\circ \leqslant \psi_\gamma \leqslant 140^\circ$, implying that the $O_\mu(K^2)$ contribution is negligibly small. However, the contribution from the $O_\mu(K^2)$ terms becomes large for ψ_γ near 0° and 180°. In fact, at $\psi_\gamma = 180^\circ$, the difference between the dashed and dotted curves is essentially half the difference between the solid and dotted curves. This shows that the $O_\mu(K^2)$ contribution is not negligible for certain ψ_γ in some cases. This analysis is based upon the following relationship between M_μ^{TuTts} (solid curve) and $M_{(1)\mu}^{\text{TuTts}}$ (dashed curve):

$$M_\mu^{\text{TuTts}} = M_{(1)\mu}^{\text{TuTts}} + O_\mu(K^2), \tag{45}$$

which implies that

$$\left|M_\mu^{\text{TuTts}}\right|^2 = \left|M_{(1)\mu}^{\text{TuTts}}\right|^2 + \Delta_2, \tag{46}$$

where

$$\Delta_2 = \left(M_{(1)\mu}^{\text{TuTts}}\right)^\dagger O^\mu(K^2) + [O^\mu(K^2)]^\dagger M_{(1)\mu}^{\text{TuTts}} + |O_\mu(K^2)|^2. \tag{47}$$

Because the solid curve is directly proportional to $|M_\mu^{\mathrm{TuTts}}|^2$ and the dashed curve is directly proportional to $|M_{(1)\mu}^{\mathrm{TuTts}}|^2$, the difference between the two must be directly proportional to Δ_2.

(c) If we use Eq. (28) and apply the same analysis, then we can investigate the contribution from $M_\mu^{(3)}(\kappa_p)$ by comparing the dashed-double-dotted curve generated using the amplitude $M_{(2)\mu}^{\mathrm{TuTts}}$ with the dotted curve corresponding to M_μ^{Low}. Similarly, if we use Eq. (29) and apply the same analysis, then we can investigate the $M_\mu^{(3)}(e)$ contribution by comparing the dashed-dotted curve generated using the amplitude $M_{(3)\mu}^{\mathrm{TuTts}}$ with the dotted curve. We should point out that the amplitude $M_\mu^{(3)}(K^1)$ is the sum of the amplitudes $M_\mu^{(3)}(e)$ and $M_\mu^{(3)}(\kappa_p)$ [see Eq. (25)]. The amplitude $M_\mu^{(3)}(e)$ is a function of the proton's Dirac magnetic moment, whereas $M_\mu^{(3)}(\kappa_p)$ is a function of the proton's anomalous magnetic moment. As shown in Fig. 5 for both the 190 and 280 MeV cases, the dashed-double-dotted curve is quantitatively similar to the dashed-dotted curve. This means that the Dirac-moment-dependent amplitude, $M_\mu^{(3)}(e)$, and the anomalous-moment-dependent amplitude, $M_\mu^{(3)}(\kappa_p)$, contribute almost equally to the $pp\gamma$ cross section.

In Figs. 6–8 we present coplanar $pp\gamma$ cross sections, calculated using M_μ^{TuTts} and M_μ^{Low}, as a function of the photon angle ψ_γ. In Fig. 6, we compare them with data at 190 MeV for proton angles $(\theta_1, \theta_2) = (16^\circ, 19^\circ)$; in Fig. 7, we do the same for $(\theta_1, \theta_2) = (8^\circ, 16^\circ)$; and in Fig. 8, at 280 MeV for proton angles $(\theta_1, \theta_2) = (12.4^\circ, 28^\circ)$. The data in Figs. 6 and 7 are from the KVI experiment [12]; in Fig. 8, from the TRIUMF experiment [13]. The solid curves correspond to $\kappa_p = 1.793$, while the dashed curves correspond to $\kappa_p = 0$. Both curves were calculated using the M_μ^{TuTts} amplitude. The dotted curves were calculated using the M_μ^{Low} amplitude with $\kappa_p = 1.793$. A comparison of the solid curves with the dashed curves demonstrates clearly that the κ_p contribution dominates the $pp\gamma$ cross sections over the entire range of ψ_γ. Because the contribution from $M_\mu^3(K^1)$ and higher-order terms $O_\mu(K^2)$ can be important in $pp\gamma$, the M_μ^{Low} amplitude [which does not include $M_\mu^3(K^1)$ and $O_\mu(K^2)$] fails to describe much of the KVI data.

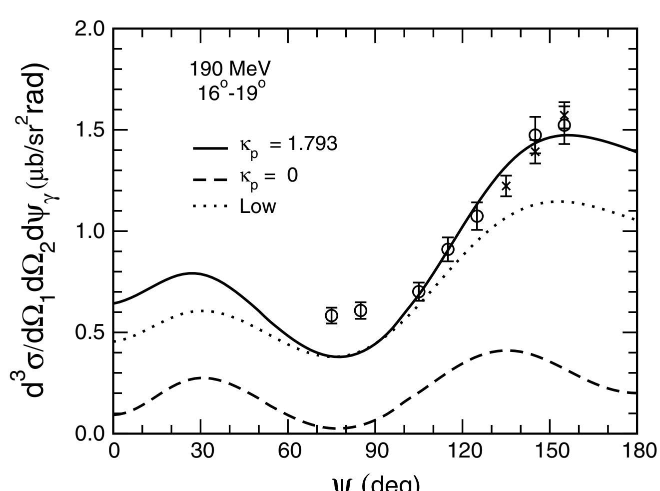

FIG. 6. Coplanar $pp\gamma$ cross sections as a function of the photon angle ψ_γ at 190 MeV for the proton scattering angles $(\theta_1, \theta_2) = (16^\circ, 19^\circ)$. Solid and dashed curves were calculated using the amplitude M_μ^{TuTts} with $\kappa_p = 1.793$ and $\kappa_p = 0$, respectively. Dotted curve was calculated using M_μ^{Low} with $\kappa_p = 1.793$. Data are from Ref. [12].

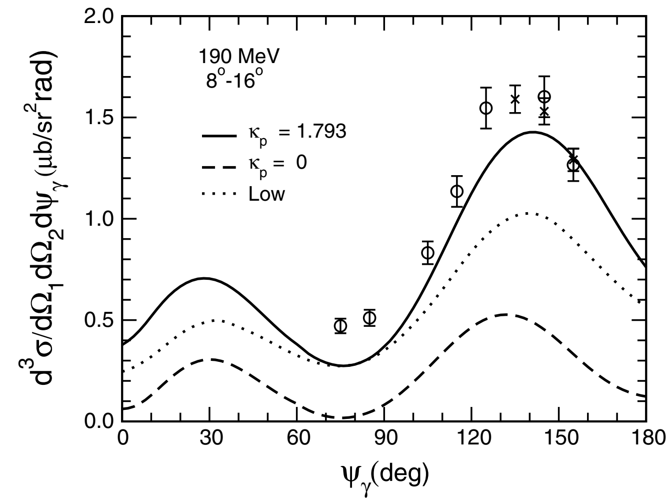

FIG. 7. Same as Fig. 6, but for $(\theta_1, \theta_2) = (8^\circ, 16^\circ)$.

As pointed out in the Introduction, the anomalous magnetic moment effect in $pp\gamma$ has been previously studied using the nonrelativistic potential model approach [1]. These studies observed that the contribution from the proton magnetic moment is significant in $pp\gamma$. For example, the most explicit demonstration of large magnetic moment effects can be seen in Fig. 8 of the paper by Brown, Anthony, and Franklin [1]. This

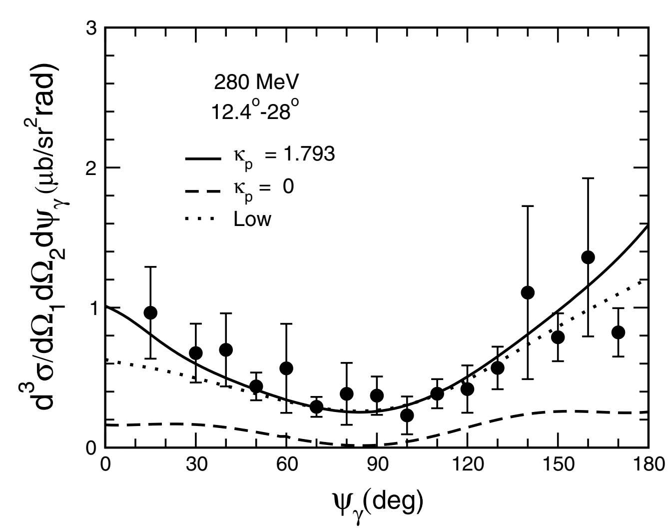

FIG. 8. Same as Fig. 6, but at 280 MeV and for $(\theta_1, \theta_2) = (12.4^\circ, 28^\circ)$. Data are from Ref. [13].

figure, which compares their calculation with the TRIUMF data, shows clearly that the contribution from the proton magnetic moment dominates the $pp\gamma$ cross section. However, an important relativistic spin correction (RSC) [14–16] was omitted in their calculation. This RSC contribution was found to be the primary relativistic correction to the magnetic term that dominates those cases involving small proton scattering angles. The large RSC effect has been reported by several groups: Workman and Fearing [17], Celenza *et al.* [18], and Herrmann and Nakayama [19]. Because of the importance of relativistic effects, we have used in our investigation a fully relativistic and gauge invariant approach.

B. $np\gamma$

The $np\gamma$ process has been systematically investigated using amplitudes $M_\mu^{\rm TuTts}$, $M_\mu^{\rm Low}$, and $M_\mu^{(1)}(K^{-1}; e)$. We investigated (i) the similarities and differences of $M_\mu^{\rm TuTts}$ and $M_\mu^{\rm Low}$, (ii) the effect of the anomalous magnetic moments κ_p and κ_n, and (iii) the meson-exchange current effect. Because the neutron and proton have unequal charges ($e_n = 0$, $e_p = e$) and anomalous magnetic moments ($\kappa_n = -1.913$, $\kappa_p = 1.793$), the emission mechanisms governing the $pp\gamma$ and $np\gamma$ processes are quite different.

(i) In Fig. 9, we present coplanar cross sections calculated using $M_\mu^{\rm TuTts}$ and $M_\mu^{\rm Low}$ as a function of photon angle ψ_γ at 200 MeV for $(\theta_n, \theta_p) = (12^\circ, 12^\circ)$, as a typical example of $np\gamma$ kinematics. The solid curve was calculated using $M_\mu^{\rm TuTts}$, while the dotted curve was calculated using $M_\mu^{\rm Low}$. In both cases, the physical values of the anomalous magnetic moments were used as input. If we compare the solid and dotted curves, then we observe that the two amplitudes predict quantitatively similar $np\gamma$ cross sections for almost all ψ_γ angles. In other words, we find

$$\left|M_\mu^{\rm TuTts}\right|^2 \simeq \left|M_\mu^{\rm Low}\right|^2. \tag{48}$$

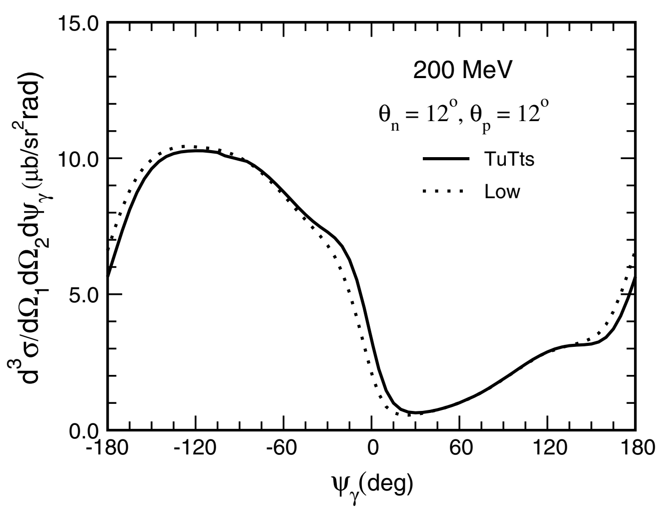

FIG. 9. Coplanar $np\gamma$ cross sections as a function of the photon angle ψ_γ at 200 MeV for the nucleon scattering angles $(\theta_n, \theta_p) = (12^\circ, 12^\circ)$. Solid and dotted curves were calculated using the amplitude $M_\mu^{\rm TuTts}$ and $M_\mu^{\rm Low}$, respectively. The anomalous magnetic moments for these calculations were $\kappa_p = 1.793$ and $\kappa_n = -1.913$.

Using the soft-photon expansion given in Eq. (24), the relationship between $|M_\mu^{\rm TuTts}|^2$ and $|M_\mu^{\rm Low}|^2$ can be expressed as

$$\left|M_\mu^{\rm TuTts}\right|^2 = \left|M_\mu^{\rm Low}\right|^2 + \Delta_3, \tag{49}$$

where

$$\begin{aligned}\Delta_3 = {} & \left(M_\mu^{\rm Low}\right)^\dagger \left[M^{(3)\mu}(K^1) + O^\mu(K^2)\right] \\ & + \left[M_\mu^{(3)}(K^1) + O_\mu(K^2)\right]^\dagger M^{{\rm Low}\mu} \\ & + \left|M_\mu^{(3)}(K^1) + O_\mu(K^2)\right|^2.\end{aligned} \tag{50}$$

Because the solid curve is directly proportional to $|M_\mu^{\rm TuTts}|^2$ while the dotted curve is directly proportional to $|M_\mu^{\rm Low}|^2$, the difference between the two must be directly proportional to Δ_3. The fact that the solid and dotted curves are consistently close to one another for most ψ_γ strongly suggests that the Δ_3 contribution is rather small. Thus, the expansion of $M_\mu^{\rm TuTts}$ given by Eq. (24) converges rapidly, and the higher-order terms $[M_\mu^{(3)}(K^1) + O_\mu(K^2)]$ should produce insignificant effects in the cross section. That is, we find

$$M_\mu^{\rm TuTts} \simeq M_\mu^{\rm Low} \tag{51}$$

for the $np\gamma$ process in the kinematics investigated.

(ii) In Figs. 10–16, we exhibit coplanar $np\gamma$ cross sections as a function of ψ_γ at 225 MeV for symmetric angle pairs $(\theta_n, \theta_p) = (32^\circ, 32^\circ)$, $(28^\circ, 28^\circ)$, $(20^\circ, 20^\circ)$, and $(12^\circ, 12^\circ)$ along with asymmetric angle pairs $(\theta_n, \theta_p) = (32^\circ, 12^\circ)$, $(32^\circ, 20^\circ)$, and $(12^\circ, 24^\circ)$. In these figures, the solid curves were calculated using the amplitude $M_\mu^{\rm TuTts}$ given by Eq. (13) with $\kappa_p = 1.793$ and $\kappa_n = -1.913$ as the anomalous magnetic moment values. The dashed-dotted curves were also calculated with $M_\mu^{\rm TuTts}$ but with

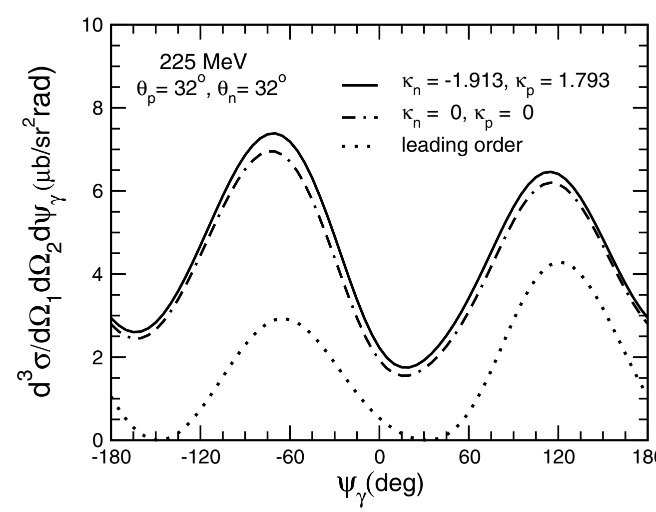

FIG. 10. Coplanar $np\gamma$ cross sections as a function of the photon angle ψ_γ at 225 MeV for the nucleon scattering angles $(\theta_n, \theta_p) = (32^\circ, 32^\circ)$. Solid curve was calculated using the amplitude $M_\mu^{\rm TuTts}$ with $\kappa_p = 1.793$ and $\kappa_n = -1.913$. Dashed-dotted curve was also calculated using $M_\mu^{\rm TuTts}$ but with $\kappa_p = \kappa_n = 0$. Dotted curve was calculated using only the leading amplitude $M_\mu^{(1)}(K^{-1}; e)$ [defined by Eq. (25) with $e_1 = 0$ and $e_2 = 1$].

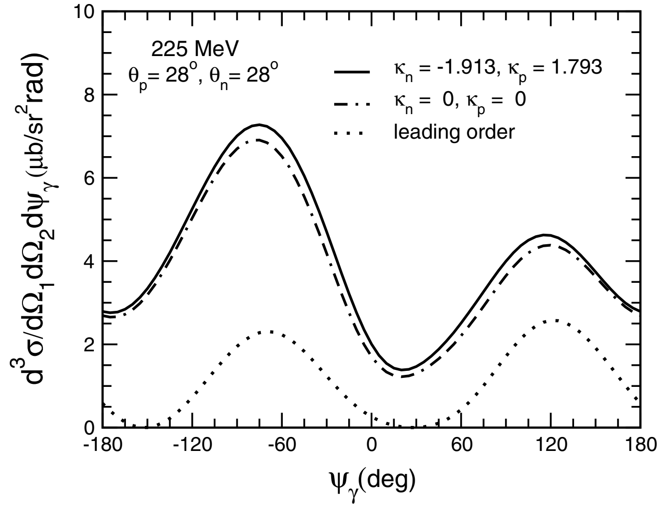

FIG. 11. Same as Fig. 10, but for $(\theta_n, \theta_p) = (28^\circ, 28^\circ)$.

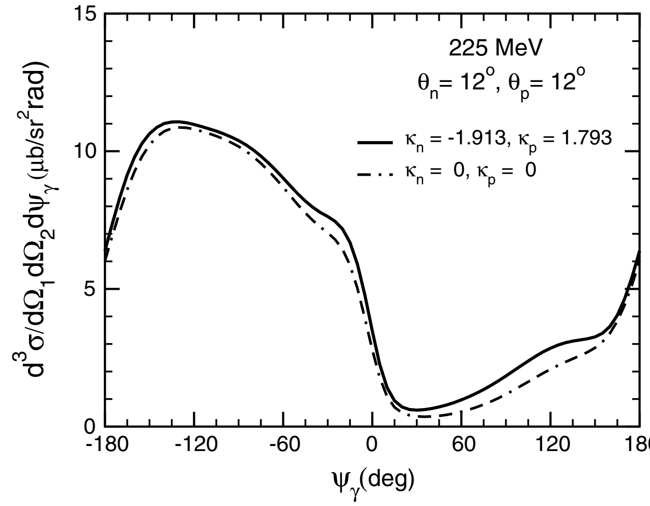

FIG. 13. Same as Fig. 10, but for $(\theta_n, \theta_p) = (12^\circ, 12^\circ)$.

$\kappa_p = \kappa_n = 0$. The dotted curves were calculated using only the amplitude $M_\mu^{(1)}(K^{-1}; e)$ as specified by Eq. (25) with $e_1 = 0$ and $e_2 = 1$. If we compare the solid curve with the dashed-dotted curve, we can ascertain that the anomalous magnetic moment contribution in each figure is negligibly small over the entire range of ψ_γ, in contrast with the $pp\gamma$ process where the contribution from such effects dominates the cross section over the entire range of ψ_γ. Therefore, the results from this investigation confirm an important finding of Ref. [3], that the anomalous magnetic moments (κ_p and κ_n) play an insignificant role in the $np\gamma$ process for the kinematics investigated.

To understand the implication of our results, we apply a similar analysis to that used in (i). Without repeating the arguments, comparison of the solid curve with the dashed-dotted curve in each of the seven figures establishes that

$$\left|M_\mu^{\text{TuTts}}\right|^2 \simeq \left|\left(M_\mu^{\text{TuTts}}\right)_{\kappa_p=\kappa_n=0}\right|^2, \tag{52}$$

which implies that

$$M_\mu^{\text{TuTts}} \simeq \left(M_\mu^{\text{TuTts}}\right)_{\kappa_p=\kappa_n=0}. \tag{53}$$

The amplitude M_μ^{Low} can be expressed as

$$\begin{aligned} M_\mu^{\text{Low}} &= M_\mu^{(1)}(K^{-1}; e) + M_\mu^{\text{mag}}(e) \\ &\quad + M_\mu^{\text{mag}}(\kappa) + M_\mu^{\text{ex}}(K^0; e). \end{aligned} \tag{54}$$

Making use of Eq. (51) and the fact that

$$\left[M_\mu^{\text{mag}}(\kappa)\right]_{\kappa_p=\kappa_n=0} = 0, \tag{55}$$

one can obtain

$$\begin{aligned} M_\mu^{\text{TuTts}} &\simeq (M_\mu^{\text{TuTts}})_{\kappa_p=\kappa_n=0} \\ &\simeq (M_\mu^{\text{Low}})_{\kappa_p=\kappa_n=0} \\ &\simeq M_\mu^{(1)}(K^{-1}; e) + M_\mu^{\text{mag}}(e) + M_\mu^{\text{ex}}(K^0; e). \end{aligned} \tag{56}$$

Equation (56) shows that the amplitude M_μ^{TuTts} is approximately equal to the sum of the three amplitudes

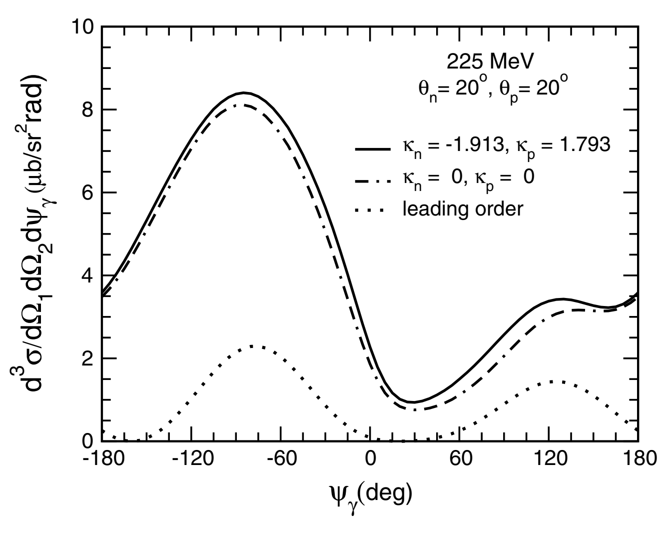

FIG. 12. Same as Fig. 10, but for $(\theta_n, \theta_p) = (20^\circ, 20^\circ)$.

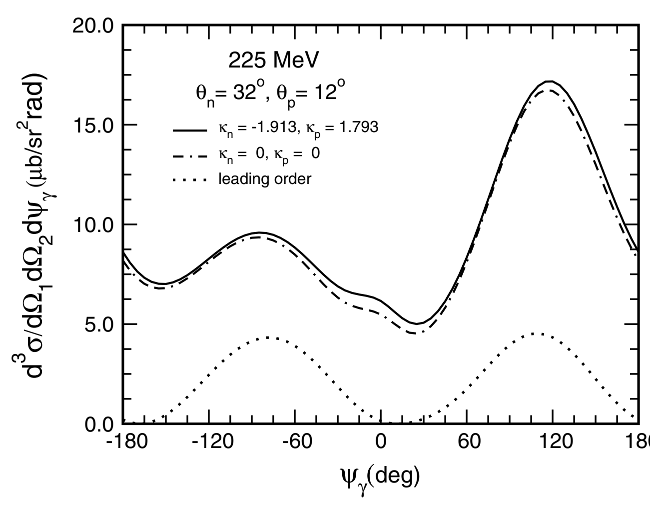

FIG. 14. Same as Fig. 10, but for $(\theta_n, \theta_p) = (32^\circ, 12^\circ)$.

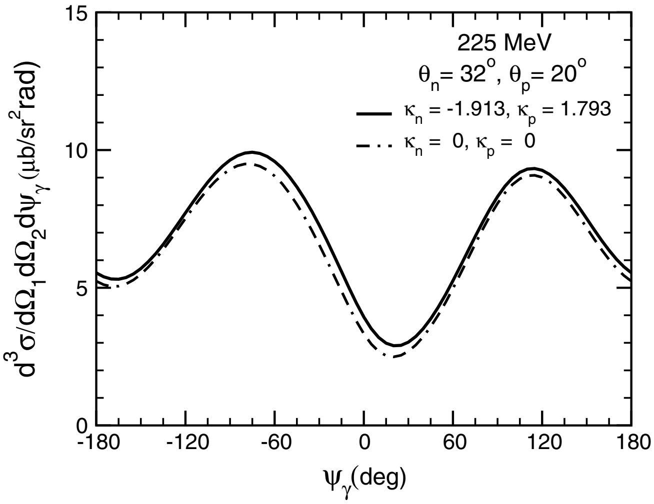

FIG. 15. Same as Fig. 10, but for $(\theta_n, \theta_p) = (32^\circ, 20^\circ)$.

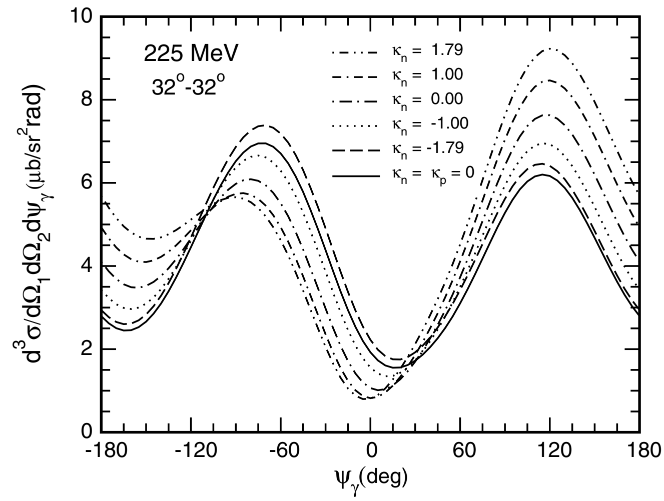

FIG. 17. Coplanar $np\gamma$ cross sections as a function of the photon angle ψ_γ at 225 MeV for the nucleon scattering angles $(\theta_n, \theta_p) = (32^\circ, 32^\circ)$. The six curves were calculated using the amplitude M_μ^{TuTts} with the same value of $\kappa_p = 1.793$, but with different values of κ_n as indicated in the figure.

$M_\mu^{(1)}(K^{-1}; e)$, $M_\mu^{\text{mag}}(e)$, and $M_\mu^{\text{ex}}(K^0; e)$. It is worthwhile to understand which of these three amplitudes makes the most important contribution.

(iii) In order to estimate the size of the contribution coming from $M_\mu^{(1)}(K^{-1}; e)$, we calculated the $np\gamma$ cross section using only that amplitude. The dotted curves in Figs. 10–16 illustrate some of the results of our calculations. In general, the contribution from $M_\mu^{(1)}(K^{-1}; e)$ is small, although not negligible, for small scattering angles (θ_n and θ_p). The contribution increases as the scattering angles approach the elastic limit.

The amplitude $M_\mu^{\text{mag}}(e)$, which is part of the magnetic amplitude, involves only the contribution from the Dirac magnetic moments. Although we have not directly investigated the contribution from this amplitude, we do not anticipate that it will make any significant contribution because: (a) the contribution coming from the other component of the magnetic amplitude, $M_\mu^{\text{mag}}(\kappa)$, which depends upon the anomalous magnetic moments κ_n and κ_p, was demonstrated to be negligibly small, and (b) we assume that the amplitude $M_\mu^{\text{mag}}(\kappa)$ and the amplitude $M_\mu^{\text{mag}}(e)$ (the Dirac-moment-dependent amplitude) contribute about equally to the $np\gamma$ cross section, just as is the case for the $pp\gamma$ process.

It is reasonable to conclude that the amplitude $M_\mu^{\text{ex}}(K^0; e)$, the exchange current amplitude, dominates the $np\gamma$ cross section if the scattering angles are small i.e., not approaching the elastic limit). That the exchange current contribution in $np\gamma$ is important is not an unknown fact [20–22]. Here, we have provided a confirmation of the effect by using a relativistic soft-photon approach.

(iv) In an effort to understand why the contribution of the anomalous magnetic moments (κ_p and κ_n) are relatively insignificant in $np\gamma$, we calculated $np\gamma$ cross sections for the physical value of $\kappa_p = 1.793$ but treated κ_n as a parameter. As shown in Fig. 17, we used the amplitude M_μ^{TuTts} to calculate cross sections for five different values of κ_n ($= -1.79, -1.00, 0, 1.00$, and 1.79). If we compare the solid curve (corresponding to $\kappa_p = \kappa_n = 0$) with the five other curves (note that the dashed-dotted curve corresponds to $\kappa_n = 0$ and $\kappa_p = 1.793$), we observe that the dashed curve is the one that is consistently closest to the solid curve. This demonstrates that the anomalous magnetic moment effects would not be negligible if the values of κ_n differed from its physical value of -1.913. In other words, the insignificant anomalous magnetic moment effect in the $np\gamma$ process may be due to a cancellation between the contribution from the anomalous magnetic moment of the proton and that of the neutron.

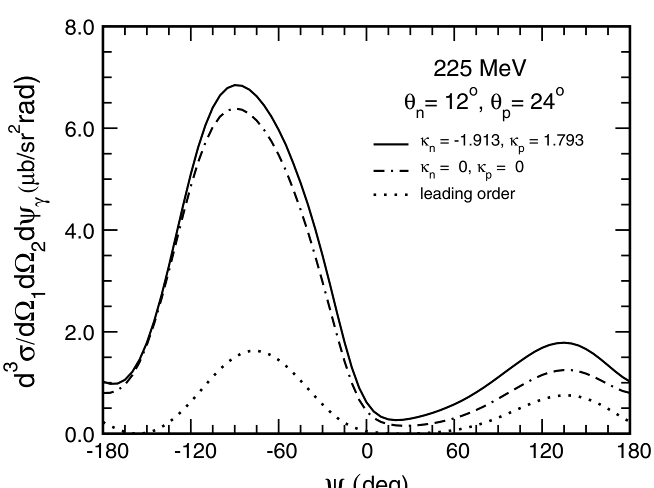

FIG. 16. Same as Fig. 10, but for $(\theta_n, \theta_p) = (12^\circ, 24^\circ)$.

C. $nn\gamma$

In Figs. 18(a) and 18(b), we present coplanar $nn\gamma$ cross sections at 190 MeV for neutron angles $(\theta_1, \theta_2) = (8^\circ, 19^\circ)$ and at 280 MeV for $(\theta_1, \theta_2) = (12.4^\circ, 12^\circ)$. These $nn\gamma$ cross

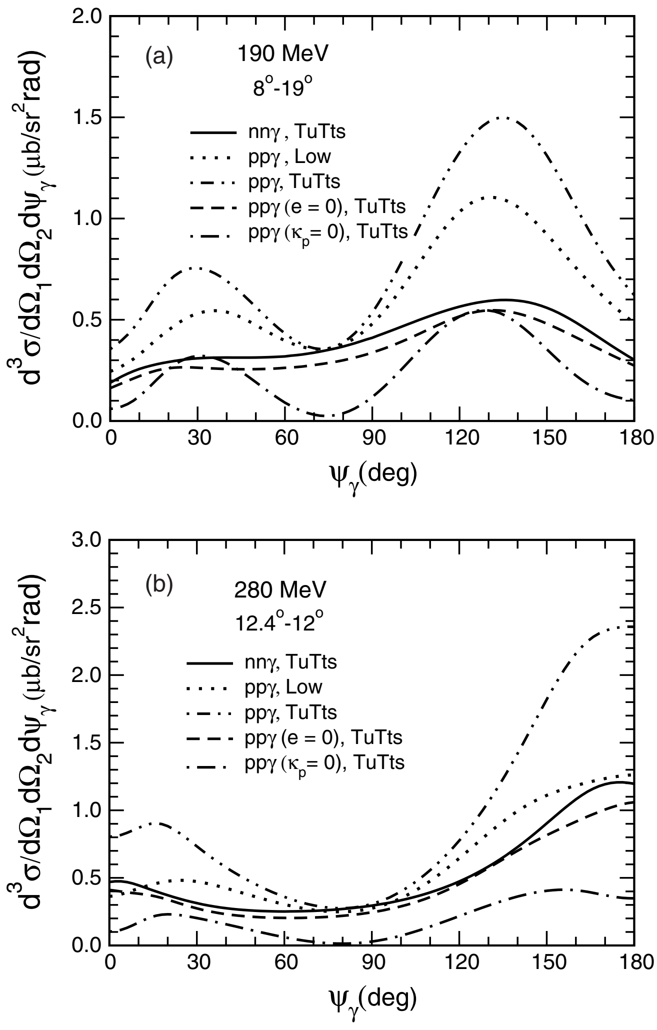

FIG. 18. Comparison of coplanar $nn\gamma$ cross sections calculated using the $M_\mu^{\mathrm{TuTts}}(nn\gamma)$ amplitude (solid curve) with $pp\gamma$ cross sections calculated using four different amplitudes: M_μ^{TuTts} (dashed-double-dotted curve), M_μ^{Low} (dotted curve), $M_{(4)\mu}^{\mathrm{TuTts}} \equiv M_\mu^{\mathrm{TuTts}}(e=0)$ (dashed curve), and $M_\mu^{\mathrm{TuTts}}(\kappa_p = 0)$ (dashed-dotted curve). All cross sections are expressed as a function of the photon angle ψ_γ at (a) 190 MeV for the neutron (proton) scattering angles $(\theta_1, \theta_2) = (8^\circ, 19^\circ)$, and (b) 280 MeV for $(\theta_1, \theta_2) = (12.4^\circ, 12^\circ)$.

sections (solid curve) were calculated using the amplitude $M_\mu^{\mathrm{TuTts}}(nn\gamma)$ given by Eq. (13) with $\kappa_n = -1.913$, and they are compared with coplanar $pp\gamma$ cross sections calculated using four different amplitudes: M_μ^{TuTts} (dashed-double-dotted curve), M_μ^{Low} (dotted curve), $M_{(4)\mu}^{\mathrm{TuTts}}$ (dashed curve), and $M_\mu^{\mathrm{TuTts}}(\kappa_p = 0)$ (dashed-dotted curve). We will focus attention on the comparison between the solid and dashed curves, because of the following interesting feature. These two curves bear a striking similarity over the entire range of ψ_γ; the solid curve is slightly higher than the dashed curve. This feature can be understood if we compare Eq. (31) with (30). From these two equations we obtain

$$\left|M_\mu^{\mathrm{TuTts}}(nn\gamma)\right|^2 = \left|M_\mu^{\mathrm{mag}}(\kappa_n) + M_\mu^{(3)}(\kappa_n)\right|^2 + \Delta_n(\kappa_n), \quad (57)$$

and

$$\left|M_{(4)\mu}^{\mathrm{TuTts}}\right|^2 = \left|M_\mu^{\mathrm{mag}}(\kappa_p) + M_\mu^{(3)}(\kappa_p)\right|^2 + \Delta_p(\kappa_p), \quad (58)$$

where

$$\begin{aligned}\Delta_n(\kappa_n) = &\left[M_\mu^{\mathrm{mag}}(\kappa_n) + M_\mu^{(3)}(\kappa_n)\right]^\dagger O^{(n)\mu}(K^2) \\ &+ [O^{(n)\mu}(K^2)]^\dagger \left[M_\mu^{\mathrm{mag}}(\kappa_n) + M_\mu^{(3)}(\kappa_n)\right] \\ &+ \left|O_\mu^{(n)}(K^2)\right|^2,\end{aligned} \quad (59)$$

and

$$\begin{aligned}\Delta_p(\kappa_p) = &\left[M_\mu^{\mathrm{mag}}(\kappa_p) + M_\mu^{(3)}(\kappa_p)\right]^\dagger O^{(p)\mu}(K^2) \\ &+ [O^{(p)\mu}(K^2)]^\dagger \left[M_\mu^{\mathrm{mag}}(\kappa_p) + M_\mu^{(3)}(\kappa_p)\right] \\ &+ \left|O_\mu^{(p)}(K^2)\right|^2.\end{aligned} \quad (60)$$

Although $\Delta_n(\kappa_n)$ is small compared with $|M_\mu^{\mathrm{mag}}(\kappa_n) + M_\mu^{(3)}(\kappa_n)|^2$, it may not be negligible for some values of ψ_γ. Similarly, $\Delta_p(\kappa_p)$ is also small compared with $|M_\mu^{\mathrm{mag}}(\kappa_p) + M_\mu^{(3)}(\kappa_p)|^2$, but it may not be negligible for some values of ψ_γ. Equation (57) shows that the $nn\gamma$ cross section calculated using $M_\mu^{\mathrm{TuTts}}(nn\gamma)$ will be approximately proportional to $|\kappa_n|^2 \simeq 3.66$, whereas Eq. (58) shows that the $pp\gamma$ cross section calculated using the amplitude $M_{(4)\mu}^{\mathrm{TuTts}}$ will be approximately proportional to $\kappa_p^2 \simeq 3.21$. Obviously, $|\kappa_n|^2$ is slightly larger than κ_p^2. Another difference between the $nn\gamma$ cross section and the $pp\gamma$ cross section is that they are calculated using different phase shifts. The phase shifts for the nn system include no Coulomb charge scattering effect, because the neutron has zero charge; whereas the phase shifts for the pp system involve Coulomb charge scattering. When the contribution from the Coulomb charge scattering effect is not significant, then the difference between the $nn\gamma$ cross section calculated using $M_\mu^{\mathrm{TuTts}}(nn\gamma)$ and the $pp\gamma$ cross section calculated using $M_{(4)\mu}^{\mathrm{TuTts}}$ will be primarily due to the difference between $|\kappa_n|^2$ and κ_p^2. This is, in fact, the situation for the results shown in Figs. 18(a) and 18(b).

Because the neutron has no charge, the amplitude $M_\mu^{\mathrm{TuTts}}(nn\gamma)$ for the $nn\gamma$ process does not involve amplitudes $M_\mu^{(1)}(K^{-1}; e)$, $M_\mu^{\mathrm{mag}}(e)$, $M_\mu^{\mathrm{ex}}(K^0; e)$, and $M_\mu^{(3)}(e)$. In other words, as shown in Eq. (31), $M_\mu^{\mathrm{TuTts}}(nn\gamma)$ can only depend upon the anomalous magnetic moment of the neutron. Moreover, the Low amplitude has a rather simple expression,

$$M_\mu^{\mathrm{Low}}(nn\gamma) = M_\mu^{\mathrm{mag}}(\kappa_n). \quad (61)$$

By using Eq. (61), Eq. (31) can be written as

$$M_\mu^{\mathrm{TuTts}}(nn\gamma) = M_\mu^{\mathrm{Low}}(nn\gamma) + M_\mu^{(3)}(\kappa_n) + O_\mu^{(n)}(\kappa^2). \quad (62)$$

Equation (62) then yields

$$\left|M_\mu^{\mathrm{TuTts}}(nn\gamma)\right|^2 = \left|M_\mu^{\mathrm{Low}}(nn\gamma)\right|^2 + \Delta_4, \quad (63)$$

where

$$\begin{aligned}\Delta_4 = &\left[M_\mu^{\mathrm{Low}}(nn\gamma)\right]^\dagger [M^{(3)\mu}(\kappa_n) + O^{(n)\mu}(K^2)] \\ &+ \left[M_\mu^{(3)}(\kappa_n) + O_\mu^{(n)}(K^2)\right]^\dagger M^{\mathrm{Low}\mu}(nn\gamma) \\ &+ \left|M_\mu^{(3)}(\kappa_n) + O_\mu^{(n)}(K^2)\right|^2.\end{aligned} \quad (64)$$

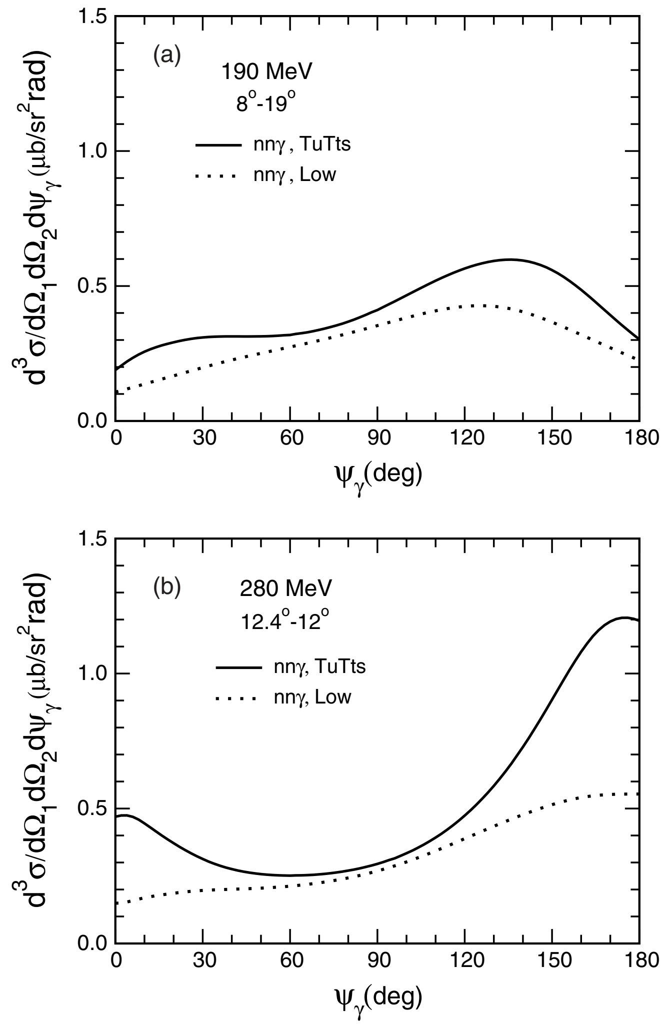

FIG. 19. Coplanar $nn\gamma$ cross sections as a function of the photon angle ψ_γ at (a) 190 MeV for the neutron scattering angles $(\theta_1, \theta_2) = (8^\circ, 19^\circ)$ and (b) 280 MeV for $(\theta_1, \theta_2) = (12.4^\circ, 12^\circ)$. Using the value of $\kappa_n = -1.913$, the solid and dotted curves were calculated from $M_\mu^{\text{TuTts}}(nn\gamma)$ and $M_\mu^{\text{Low}}(nn\gamma)$, respectively.

Equations (63) and (64) show that if we use amplitudes $M_\mu^{\text{TuTts}}(nn\gamma)$ and $M_\mu^{\text{Low}}(nn\gamma)$ to calculate $nn\gamma$ cross sections, then the contribution from $M_\mu^{(3)}(\kappa_n)$ and $O_\mu^{(n)}(K^2)$ can be investigated. In Figs. 19(a) and 19(b), we present coplanar $nn\gamma$ cross sections at 190 MeV for $(\theta_1, \theta_2) = (8^\circ, 19^\circ)$ and at 280 MeV for $(\theta_1, \theta_2) = (12.4^\circ, 12^\circ)$. The solid curves were generated using the amplitude $M_\mu^{\text{TuTts}}(nn\gamma)$ given by Eq. (13) [or Eq. (62)] with $\kappa_n = -1.913$, while the dotted curves were generated using the amplitude $M_\mu^{\text{Low}}(nn\gamma)$ given by Eq. (61) using the same value of κ_n. From Eq. (63), it is clear that the difference between the solid and dotted curves is directly proportional to Δ_4. Figures 19(a) and 19(b) clearly demonstrate that the contribution from Δ_4 can be significant for most photon angles ψ_γ, especially for the case of 280 MeV near $\psi_\gamma = 0^\circ$ and 180°. This implies that the contribution from $M_\mu^{(3)}(\kappa_n)$ and $O_\mu^{(n)}(\kappa^2)$ is indeed important for the $nn\gamma$ process in the kinematic region investigated. Moreover, this explains why the amplitude $M_\mu^{\text{TuTts}}(nn\gamma)$ should be used to describe the $nn\gamma$ process.

IV. CONCLUSIONS

In brief, we have systematically investigated nucleon-nucleon bremsstrahlung processes using the two-u-two-t special amplitude M_μ^{TuTts} and the Low amplitude M_μ^{Low}. With the help of the special soft-photon expansion given by Eq. (24), we have analyzed the relationship between M_μ^{TuTts} and M_μ^{Low} both analytically and numerically. The essential difference between these two amplitudes is that M_μ^{TuTts} includes an amplitude $M_\mu^{(3)}(K^1)$ which is of order K. For both $pp\gamma$ and $np\gamma$ processes, the additional amplitude $M_\mu^{(3)}(K^1)$ involves the Dirac-moment-dependent amplitude $M_\mu^{(3)}(e)$ and the anomalous-moment-dependent amplitude $M_\mu^{(3)}(\kappa)$. However, for the $nn\gamma$ process, $M_\mu^{(3)}(K^1)$ depends only upon the anomalous-moment-dependent amplitude $M_\mu^{(3)}(\kappa)$. We have demonstrated that the contribution of $M_\mu^{(3)}(K^1)$ can be significant in $pp\gamma$ and $nn\gamma$ for the kinematics investigated, even though such a contribution was found to be essentially negligible in $np\gamma$. Moreover, our calculation shows that $M_\mu^{(3)}(e)$ and $M_\mu^{(3)}(\kappa)$ contribute almost equally to the $pp\gamma$ cross section.

The primary focus of this work has been the investigation of the κ_p and κ_n contributions to the $pp\gamma, np\gamma$, and $nn\gamma$ processes. For the $pp\gamma$ process at small scattering angles $(\theta_1 < 25^\circ, \theta_2 < 25^\circ)$ at $E_i \geqslant 150\,\text{MeV}$, the κ_p contribution dominates the $pp\gamma$ cross-section over the entire range of ψ_γ. In fact, the contribution is sufficiently important that the amplitude $M_\mu^{(3)}(K)$ cannot be neglected in $pp\gamma$ cross-section calculations. Therefore, in the description of the $pp\gamma$ cross-section data, the M_μ^{TuTts} amplitude is a better approximation than is the M_μ^{Low} amplitude. In contrast, for the same $pp\gamma$ process with scattering angles approaching the elastic limit $(\theta_1 \geqslant 40^\circ, \theta_2 \geqslant 40^\circ)$, the κ_p contribution becomes negligibly small, and the two κ_p-dependent amplitudes $[M_\mu^{\text{mag}}(\kappa_p)$ and $M_\mu^{(3)}(\kappa_p)]$ can be ignored. In this case, the amplitudes M_μ^{TuTts} and M_μ^{Low} predict almost equal $pp\gamma$ cross sections. For the $np\gamma$ process, because the anomalous magnetic moments κ_p and κ_n play an insignificant role, the amplitudes $M_\mu^{\text{mag}}(\kappa)$ and $M_\mu^{(3)}(\kappa)$ are essentially negligible. Moreover, we have found that the amplitude $M_\mu^{(3)}(K^1)$ $[= M_\mu^{(3)}(e) + M_\mu^{(3)}(\kappa)]$ along with the higher-order terms $[O_\mu(K^2)]$ produce insignificant effects in the $np\gamma$ cross section. Thus, M_μ^{TuTts} and M_μ^{Low} are approximately equivalent, and the two amplitudes predict quantitatively similar $np\gamma$ cross sections. Our study reveals that the insignificant anomalous magnetic moment effect may be due to a cancellation between contributions from κ_p and κ_n. Our investigation also demonstrates that the amplitude $M_\mu^{\text{ex}}(K^0; e)$, which involves meson-exchange current contributions, dominates the $np\gamma$ cross sections. Results from an $nn\gamma$ investigation are reported for the first time. Because the $M_\mu^{(3)}(\kappa_n)$ amplitude contribution is significant, M_μ^{TuTts} and M_μ^{Low} predict quite different $nn\gamma$ cross sections. There is a striking similarity between the $nn\gamma$ cross section using the amplitude M_μ^{TuTts} and the $pp\gamma$ cross section calculated using the $M_{(4)\mu}^{\text{TuTts}}$ amplitude. The reason for such a similarity was discussed.

In conclusion, our findings have enhanced the understanding of the fundamental emission mechanism governing the $NN\gamma$ processes. Our results show that the amplitude M_μ^{TuTts} should be used to describe all three $NN\gamma$ processes. Nonetheless, a complete understanding of the $NN\gamma$ processes requires additional exploration of exchange current effects and anomalous magnetic moment effects such as form factor contributions from the $N\gamma N$ vertices.

ACKNOWLEDGMENTS

The work of M.K.L. was supported in part by the CUNY Professional Staff Congress, Board of Higher Education Research Award Program. The work of B.F.G. was supported by the U.S. Department of Energy under Contract W-7405-ENG-36.

APPENDIX A: DERIVATION OF THE M_μ^{TuTts} AMPLITUDE FOR THE $np\gamma$ AND $nn\gamma$ PROCESSES

The M_μ^{TuTts} amplitude differs from the M_μ^{Low} amplitude. The primary difference lies in the different on-shell kinematic points at which the two amplitudes are evaluated. Therefore, the procedure for deriving the two amplitudes differ to some extent. In this Appendix, the derivation of the M_μ^{TuTts} amplitude for both $np\gamma$ and $nn\gamma$ processes is briefly outlined. Special attention will be paid to the derivation of the internal amplitude, because such a derivation is new. Moreover, the external amplitude is unique and well known.

1. The M_μ^{TuTts} amplitude for the $np\gamma$ process

The external amplitude M_μ^E is a sum of four different half-off-shell amplitudes,

$$M_\mu^E = M_\mu^{P_1}(u_2, t_2, \Delta_{P_1}) + M_\mu^{P_1'}(u_1, t_2, \Delta_{P_1'}) + M_\mu^{P_2}(u_1, t_1, \Delta_{P_2}) + M_\mu^{P_2'}(u_2, t_1, \Delta_{P_2'}), \quad \text{(A1)}$$

where

$$\begin{aligned}
M_\mu^{P_1}(u_2, t_2, \Delta_{P_1}) &= e\sum_{\alpha=1}^{5} F_\alpha^e(u_2, t_2, \Delta_{P_1})\bar{u}(P_1') \times \lambda_\alpha \frac{1}{\not P_1 - \not K - m}\Gamma_\mu^n u(P_1)U^\alpha(2),\\
M_\mu^{P_1'}(u_1, t_2, \Delta_{P_1'}) &= e\sum_{\alpha=1}^{5} F_\alpha^e(u_1, t_2, \Delta_{P_1'})\bar{u}(P_1') \times \Gamma_\mu^n \frac{1}{\not P_1' + \not K - m}\lambda_\alpha u(P_1)U^\alpha(2),\\
M_\mu^{P_2}(u_1, t_1, \Delta_{P_2}) &= e\sum_{\alpha=1}^{5} F_\alpha^e(u_1, t_1, \Delta_{P_2})U_\alpha(1)\bar{u}(P_2') \times \lambda^\alpha \frac{1}{\not P_2 - \not K - m}\Gamma_\mu^p u(P_2),\\
M_\mu^{P_2'}(u_2, t_1, \Delta_{P_2'}) &= e\sum_{\alpha=1}^{5} F_\alpha^e(u_2, t_1, \Delta_{P_2'})U_\alpha(1)\bar{u}(P_2') \times \Gamma_\mu^p \frac{1}{\not P_2' + \not K - m}\lambda^\alpha u(P_2),
\end{aligned} \quad \text{(A2)}$$

and we have defined

$$\begin{aligned}
U^\alpha(j) &= \bar{u}(P_j')\lambda^\alpha u(P_j), \quad (j = 1, 2)\\
\Gamma_\mu^p &= \gamma_\mu - i\frac{\kappa_p}{2m}\sigma_{\mu\nu}K^\nu,\\
\Gamma_\mu^n &= -i\frac{\kappa_n}{2m}\sigma_{\mu\nu}K^\nu,\\
\Delta_{P_1} &= (P_1 - K)^2 = m^2 - 2P_1\cdot K,\\
\Delta_{P_1'} &= (P_1' + K)^2 = m^2 + 2P_1'\cdot K,\\
\Delta_{P_2} &= (P_2 - K)^2 = m^2 - 2P_2\cdot K,\\
\Delta_{P_2'} &= (P_2' + K)^2 = m^2 + 2P_2'\cdot K.
\end{aligned}$$

Four different off-shell kinematic conditions, which specify the four amplitudes $M_\mu^{P_x}$ ($P_x = P_1, P_1', P_2, P_2'$), are given by Eq. (16). In terms of the external amplitude M_μ^E given by Eq. (A1), the internal amplitude M_μ^I can be obtained from the gauge invariance condition

$$\left(M_\mu^E + M_\mu^I\right)K^\mu = 0. \quad \text{(A3)}$$

To derive the leading term of the amplitude M_μ^I, which is valid to the K^0 order, one must impose on-shell conditions which define on-shell points and then expand the amplitude M_μ^E about these on-shell points—the soft-photon expansion. Because different prescriptions impose different on-shell conditions, different versions of the internal amplitude M_μ^I can be obtained from Eq. (A3). The Low prescription, which has been used to derive the Low amplitude, is a typical example. This prescription imposes the single common on-shell condition given by Eq. (21), which defines the single on-shell point $(\bar{u}, \bar{t}, m^2)$ [or $(\bar{s}, \bar{t}, m^2)$], for all half-off-shell amplitudes $M_\mu^{P_1}(u_2, t_2, \Delta_{P_1})$, $M_\mu^{P_1'}(u_1, t_2, \Delta_{P_1'})$, $M_\mu^{P_2}(u_1, t_1, \Delta_{P_2})$, and $M_\mu^{P_2'}(u_2, t_1, \Delta_{P_2'})$. If one expands all amplitudes $M_\mu^{P_x}$ ($P_x = P_1, P_1', P_2, P_2'$) about the common on-shell point $(\bar{u}, \bar{t}, m^2)$, then the internal amplitude M_μ^I, valid to the K^0 order, can be constructed from Eq. (A3). The resulting Low amplitude M_μ^{Low} ($= M_\mu^E + M_\mu^I$, valid to the K^0 order) will depend upon the elastic scattering amplitude and its derivatives evaluated at $(\bar{u}, \bar{t})$ [or $(\bar{s}, \bar{t})$]. Such a Low amplitude for the $np\gamma$ process was first derived by Nyman [8]. Here, we will focus upon the derivation of the amplitude M_μ^{TuTts}. We follow the procedure employed in Ref. [5], the difference being that we treat the $np\gamma$ case rather than the $pp\gamma$ case.

In deriving the M_μ^{TuTts} amplitude, one imposes the four on-shell conditions given by Eq. (17), which define four different on-shell points. Therefore, to obtain M_μ^I from Eq. (A3), one must expand components of the amplitude M_μ^E given by Eq. (A1) about the four separate on-shell points; that is,

(i) expand the amplitude $M_\mu^{P_1}(u_2, t_2, \Delta_{P_1})$ or $F_\alpha^e(u_2, t_2, \Delta_{P_1})$ about the on-shell point (u_2, t_2, m^2),

(ii) expand the amplitude $M_\mu^{P_1'}(u_1, t_2, \Delta_{P_1'})$ or $F_\alpha^e(u_1, t_2, \Delta_{P_1'})$ about the on-shell point (u_1, t_2, m^2),
(iii) expand the amplitude $M_\mu^{P_2}(u_1, t_1, \Delta_{P_2})$ or $F_\alpha^e(u_1, t_1, \Delta_{P_2})$ about the on-shell point (u_1, t_1, m^2), and
(iv) expand the amplitude $M_\mu^{P_2'}(u_2, t_1, \Delta_{P_2'})$ or $F_\alpha^e(u_2, t_1, \Delta_{P_2'})$ about the on-shell point (u_2, t_1, m^2).

One obtains the following expansion (up to the K^0 order):

$$\begin{aligned} M_\mu^E = e\sum_{\alpha=1}^{5}\Bigg\{&\bar{u}(P_1')\left[F_\alpha^e(u_1,t_2)\left(\frac{R_\mu^{P_1'}}{P_1'\cdot K}\right)\lambda_\alpha\right.\\ &\left.-F_\alpha^e(u_2,t_2)\lambda_\alpha\left(\frac{R_\mu^{P_1}}{P_1\cdot K}\right)\right]u(P_1)U^\alpha(2)\\ &+U_\alpha(1)\bar{u}(P_2')\left[F_\alpha^e(u_2,t_1)\left(\frac{P_{2\mu}'+R_\mu^{P_2'}}{P_2'\cdot K}\right)\lambda^\alpha\right.\\ &\left.-F_\alpha^e(u_1,t_1)\lambda^\alpha\left(\frac{P_{2\mu}+R_\mu^{P_2}}{P_2\cdot K}\right)\right]\\ &\times u(P_2)+D_{\alpha\mu}U_\alpha(1)U^\alpha(2)\Bigg\}, \end{aligned} \tag{A4}$$

where

$$\begin{aligned} D_{\alpha\mu} &= (2P_{2\mu})\left[\frac{\partial F_\alpha^e(u_1,t_1,\Delta_{P_2})}{\partial\Delta_{P_2}}\right]_{\Delta_{P_2}=m^2}\\ &\quad+(2P_{2\mu}')\left[\frac{\partial F_\alpha^e(u_2,t_1,\Delta_{P_2'})}{\partial\Delta_{P_2'}}\right]_{\Delta_{P_2'}=m^2}, \end{aligned}$$

$$\begin{aligned} F_\alpha^e(u_1,t_2) &\equiv F_\alpha^e(u_1,t_2,m^2),\\ F_\alpha^e(u_2,t_2) &\equiv F_\alpha^e(u_2,t_2,m^2),\\ F_\alpha^e(u_2,t_1) &\equiv F_\alpha^e(u_2,t_1,m^2),\\ F_\alpha^e(u_1,t_1) &\equiv F_\alpha^e(u_1,t_1,m^2),\\ R_\mu^{Q_1} &= \frac{\kappa_n}{8m}\{[\gamma_\mu,\not{K}],\not{Q}_1\},\quad (Q_1=P_1,P_1')\\ R_\mu^{Q_2} &= \frac{1}{4}[\gamma_\mu,\not{K}]+\frac{\kappa_p}{8m}\{[\gamma_\mu,\not{K}],\not{Q}_2\},\quad (Q_2=P_2,P_2') \end{aligned}$$

and we have used $[A,B]\equiv AB-BA$ and $\{A,B\}\equiv AB+BA$. Substituting Eq. (A4) into Eq. (A3), one finds

$$\begin{aligned} M_\mu^I K^\mu &= -M_\mu^E K^\mu\\ &= -e\sum_{\alpha=1}^{5}[I_\alpha+D_{\alpha\mu}K^\mu]U_\alpha(1)U^\alpha(2), \end{aligned} \tag{A5}$$

where

$$I_\alpha = F_\alpha^e(u_2,t_1)-F_\alpha^e(u_1,t_1). \tag{A6}$$

One can rewrite I_α in the following manner,

$$\begin{aligned} I_\alpha = \tfrac{1}{2}\big\{&\big[F_\alpha^e(u_2,t_1)-F_\alpha^e(u_2,t_2)\big]\\ &+\big[F_\alpha^e(u_1,t_2)-F_\alpha^e(u_1,t_1)\big]\\ &+\big[F_\alpha^e(u_2,t_2)-F_\alpha^e(u_1,t_2)\big]\\ &+\big[F_\alpha^e(u_2,t_1)-F_\alpha^e(u_1,t_1)\big]\big\}. \end{aligned} \tag{A7}$$

Applying the mean-value theorem to Eq. (A7), one obtains

$$\begin{aligned} I_\alpha = &-(P_2-P_2')\cdot K\,\frac{\partial F_\alpha^e(u_2,t_m')}{\partial t_m'}\\ &+(P_2-P_2')\cdot K\,\frac{\partial F_\alpha^e(u_1,t_m)}{\partial t_m}\\ &-(P_1-P_2')\cdot K\,\frac{\partial F_\alpha^e(u_m,t_2)}{\partial u_m}\\ &-(P_1-P_2')\cdot K\,\frac{\partial F_\alpha^e(u_m',t_1)}{\partial u_m'}, \end{aligned} \tag{A8}$$

where t_m and t_m' lie between t_1 and t_2, and u_m and u_m' lie between u_1 and u_2. Inserting Eq. (A8) into Eq. (A5), one can determine M_μ^I to be

$$\begin{aligned} M_\mu^I = -e\sum_{\alpha=1}^{5}\Bigg[&-(P_2-P_2')_\mu\frac{\partial F_\alpha^e(u_2,t_m')}{\partial t_m'}\\ &+(P_2-P_2')_\mu\,\frac{\partial F_\alpha^e(u_1,t_m)}{\partial t_m}\\ &-(P_1-P_2')_\mu\,\frac{\partial F_\alpha^e(u_m,t_2)}{\partial u_m}\\ &-(P_1-P_2')_\mu\frac{\partial F_\alpha^e(u_m',t_1)}{\partial u_m'}+D_{\alpha\mu}\Bigg]U_\alpha(1)U^\alpha(2). \end{aligned} \tag{A9}$$

Again, using the mean-value theorem, one can replace the derivatives of F_α^e with respect to t_m', t_m, u_m, and u_m' by the finite differences of Eq. (A7) to obtain

$$\begin{aligned} M_\mu^I = -\frac{e}{2}\sum_{\alpha=1}^{5}\Bigg\{&\frac{(P_2-P_2')_\mu}{(P_2-P_2')\cdot K}\big[F_\alpha^e(u_2,t_1)-F_\alpha^e(u_2,t_2)\big]\\ &+\frac{(P_2-P_2')_\mu}{(P_2-P_2')\cdot K}\big[F_\alpha^e(u_1,t_2)-F_\alpha^e(u_1,t_1)\big]\\ &+\frac{(P_1-P_2')_\mu}{(P_1-P_2')\cdot K}\big[F_\alpha^e(u_2,t_2)-F_\alpha^e(u_1,t_2)\big]\\ &+\frac{(P_1-P_2')_\mu}{(P_1-P_2')\cdot K}\big[F_\alpha^e(u_2,t_1)-F_\alpha^e(u_1,t_1)\big]\\ &+2D_{\alpha\mu}\Bigg\}U_\alpha(1)U^\alpha(2) \end{aligned} \tag{A10}$$

$$\begin{aligned} = -e\sum_{\alpha=1}^{5}\big[&-V_\mu'F_\alpha^e(u_2,t_2)+V_\mu F_\alpha^e(u_2,t_1)\\ &+V_\mu'F_\alpha^e(u_1,t_2)-V_\mu F_\alpha^e(u_1,t_1)\\ &+D_{\alpha\mu}\big]U_\alpha(1)U^\alpha(2), \end{aligned} \tag{A11}$$

where

$$V_\mu = \frac{(P_1-P_2')_\mu}{2(P_1-P_2')\cdot K}+\frac{(P_2-P_2')_\mu}{2(P_2-P_2')\cdot K}, \tag{A12}$$

$$V_\mu' = \frac{(P_2-P_2')_\mu}{2(P_2-P_2')\cdot K}-\frac{(P_1-P_2')_\mu}{2(P_1-P_2')\cdot K}. \tag{A13}$$

The amplitude M_μ^{TuTts} for the $np\gamma$ process can be obtained by combining the external amplitude M_μ^E of Eq. (A4) with the internal amplitude M^I_μ of Eq. (A11),

$$M^T_\mu = M^E_\mu + M^I_\mu = M^{\mathrm{TuTts}}_\mu + O(K). \tag{A14}$$

The explicit expression for M^{TuTts}_μ is given by Eq. (13).

2. The amplitude M^{TuTts}_μ for the $nn\gamma$ process

The external amplitude M^E_μ is a sum of four different half-off-shell amplitudes,

$$\begin{aligned} M^E_\mu = {} & M^{P_1}_\mu(u_2, t_2, \Delta_{P_1}) + M^{P_1'}_\mu(u_1, t_2, \Delta_{P_1'}) \\ & + \bar{M}^{P_2}_\mu(u_1, t_1, \Delta_{P_2}) + \bar{M}^{P_2'}_\mu(u_2, t_1, \Delta_{P_2'}), \end{aligned} \tag{A15}$$

where

$$\begin{aligned} M^{P_1}_\mu(u_2, t_2, \Delta_{P_1}) &= e\sum_{\alpha=1}^{5} F^e_\alpha(u_2, t_2, \Delta_{P_1})\bar{u}(P_1') \\ &\quad \times \lambda_\alpha \frac{1}{\not{P}_1 - \not{K} - m}\Gamma^n_\mu u(P_1)U^\alpha(2), \\ M^{P_1'}_\mu(u_1, t_2, \Delta_{P_1'}) &= e\sum_{\alpha=1}^{5} F^e_\alpha(u_1, t_2, \Delta_{P_1'})\bar{u}(P_1') \\ &\quad \times \Gamma^n_\mu \frac{1}{\not{P}_1' + \not{K} - m}\lambda_\alpha u(P_1)U^\alpha(2), \end{aligned} \tag{A16}$$

$$\begin{aligned} \bar{M}^{P_2}_\mu(u_1, t_1, \Delta_{P_2}) &= e\sum_{\alpha=1}^{5} F^e_\alpha(u_1, t_1, \Delta_{P_2})U_\alpha(1)\bar{u}(P_2') \\ &\quad \times \lambda^\alpha \frac{1}{\not{P}_2 - \not{K} - m}\Gamma^n_\mu u(P_2), \\ \bar{M}^{P_2'}_\mu(u_2, t_1, \Delta_{P_2'}) &= e\sum_{\alpha=1}^{5} F^e_\alpha(u_2, t_1, \Delta_{P_2'})U_\alpha(1)\bar{u}(P_2') \\ &\quad \times \Gamma^n_\mu \frac{1}{\not{P}_2' + \not{K} - m}\lambda^\alpha u(P_2). \end{aligned}$$

Some of the symbols used here were defined in Eq. (A2). It is obvious that the four different off-shell kinematic conditions [Eq. (16)] which specify the four amplitudes $M^{P_x}_\mu(P_x = P_1, P_1', P_2, P_2')$ should apply to all three $NN\gamma$ processes. If we impose the on-shell points (u_2, t_2, m^2), (u_1, t_2, m^2), (u_1, t_1, m^2), and (u_2, t_1, m^2) upon the amplitudes $M^{P_1}_\mu(u_2, t_2, \Delta_{P_1})$, $M^{P_1'}_\mu(u_1, t_2, \Delta_{P_1'})$, $M^{P_2}_\mu(u_1, t_1, \Delta_{P_2})$, and $M^{P_2'}_\mu(u_2, t_1, \Delta_{P_2'})$, respectively, then the external amplitude M^E_μ has the following expansion up to the K^0 order:

$$\begin{aligned} M^E_\mu = e\sum_{\alpha=1}^{5} \Bigg\{ & \bar{u}(P_1')\left[F^e_\alpha(u_1, t_2)\left(\frac{\bar{R}^{P_1'}_\mu}{P_1'\cdot K}\right)\lambda_\alpha \right. \\ & \left. - F^e_\alpha(u_2, t_2)\lambda_\alpha\left(\frac{\bar{R}^{P_1}_\mu}{P_1\cdot K}\right)\right]u(P_1)U^\alpha(2) \\ & + U_\alpha(1)\bar{u}(P_2')\left[F^e_\alpha(u_2, t_1)\left(\frac{\bar{R}^{P_2'}_\mu}{P_2'\cdot K}\right)\lambda^\alpha \right. \\ & \left. - F^e_\alpha(u_1, t_1)\lambda^\alpha\left(\frac{\bar{R}^{P_2}_\mu}{P_2\cdot K}\right)\right]u(P_2)\Bigg\}, \end{aligned} \tag{A17}$$

where

$$\bar{R}^{P_x} = \frac{\kappa_n}{8m}\{[\gamma_\mu, \not{K}], \not{P}_x\},\ (P_x = P_1, P_1', P_2, P_2').$$

Because the amplitudes $M^{P_x}_\mu(P_x = P_1, P_1', P_2, P_2')$ are separately gauge invariant, we have

$$M^E_\mu K^\mu = 0. \tag{A18}$$

From the gauge invariance condition, we also have

$$M^I_\mu K^\mu = -M^E_\mu K^\mu = 0.$$

The simplest choice for K^I_μ is to take

$$M^I_\mu = 0 \tag{A19}$$

and

$$M^{\mathrm{TuTts}}_\mu = M^E_\mu,$$

where M^E_μ is given in Eq. (A17). This is why the expression for the amplitude M^{TuTts}_μ in Eq. (13) for the $nn\gamma$ process has the same form as the amplitude M^E_μ given by Eq. (A17).

[1] See, for example, H. W. Fearing, in *Nucleon-Nucleon Interactions—1977*, edited by D. Measday, H. Fearing, and A. Strathdee, AIP Conf. Proc. No. 41 (AIP, New York, 1978), p. 506; V. R. Brown, P. L. Anthony, and J. Franklin, Phys. Rev. C **44**, 1296 (1991). See also the discussion appearing at the end of the $pp\gamma$ results Sec. III A. Note that in some papers, the data quoted from Ref. [13] have been multipled by 3/2.

[2] F. E. Low, Phys. Rev. **110**, 974 (1958).

[3] M. K. Liou, T. D. Penninga, R. G. E. Timmermans, and B. F. Gibson, Phys. Rev. C **69**, 011001(R) (2004).

[4] M. L. Goldberger, M. T. Grisaru, S. W. Macdowell, and D. Y. Wong, Phys. Rev. **120**, 2250 (1960).

[5] M. K. Liou, R. Timmermans, and B. F. Gibson, Phys. Rev. C **54**, 1574 (1996).

[6] R. G. E. Timmermans, B. F. Gibson, Yi Li, and M. K. Liou, Phys. Rev. C **65**, 014001 (2001).

[7] M. K. Liou, D. Lin, and B. F. Gibson, Phys. Rev. C **47**, 973 (1993).

[8] E. M. Nyman, Phys. Rev. **170**, 1628 (1968).

[9] V. G. J. Stoks, R. A. M. Klomp, M. C. M. Rentmeester, and J. J. de Swart, Phys. Rev. C **48**, 792 (1993); http://nn-online.org.

[10] M. C. M. Rentmeester, R. G. E. Timmermans, J. L. Friar, and J. J. de Swart, Phys. Rev. Lett. **82**, 4992 (1999); M. C. M. Rentmeester, R. G. E. Timmermans, and J. J. de Swart, Phys. Rev. C **67**, 044001 (2003).

[11] B. Gottschalk, W. J. Shlaer, and K. H. Wang, Nucl. Phys. **A94**, 491 (1967).

[12] H. Huisman *et al.*, Phys. Rev. Lett. **83**, 4017 (1999); Phys. Lett. **B476**, 9 (2000); Phys. Rev. C **65**, 031001(R) (2002); M. Mahjour-Shafiei *et al.*, *ibid.* **70**, 024004 (2004).
[13] K. Michaelian *et al.*, Phys. Rev. D **41**, 2689 (1990).
[14] J. H. McGuire, Phys. Lett. **B32**, 73 (1970).
[15] M. K. Liou and K. S. Cho, Nucl. Phys. **A160**, 417 (1971).
[16] M. K. Liou and M. I. Sobel, Ann. Phys. (NY) **72**, 323 (1972).
[17] R. L. Workman and H. W. Fearing, Phys. Rev. C **34**, 780 (1986).
[18] L. S. Celenza, M. K. Liou, M. I. Sobel, and B. F. Gibson, Phys. Rev. C **8**, 838 (1973).
[19] V. Herrmann and K. Nakayama, Phys. Rev. C **46**, 2199 (1992).
[20] V. R. Brown and J. Franklin, Phys. Rev. C **8**, 1706 (1973).
[21] K. Nakayama, Phys. Rev. C **39**, 1475 (1989).
[22] V. Herrmann, J. Speth, and K. Nakayama, Phys. Rev. C **43**, 394 (1991).